

Analysis of CO₂ storage efficiency and performance of low carbon cement binders containing carbide slag and phosphorus slag

Guang-Min Liu^{b,1}, Rui-Cong Gao^{b,1}, Fang Liu^a, Wen-Ping Yue^a, Yi Yang^{a,*}, Yong-Pang Liao^b, Jia-Xiang Liew^{c,*}

^a Shaanxi Key Laboratory of Safety and Durability of Concrete Structures, Xijing University, Xi'an 710123, China

^b International Joint Laboratory for Green Construction and Intelligent Maintenance of Yunnan Province, Faculty of Civil Engineering and Mechanics, Kunming University of Science and Technology, Kunming 650500, China

^c Department of Civil and Environmental Engineering, The Hong Kong Polytechnic University, Kowloon, Hong Kong

ARTICLE INFO

Keywords:

Phosphorus slag
Carbide slag
Carbonation curing
Normal curing
Synergistic effect

ABSTRACT

Phosphorus slag (PS) and carbide slag (CS) are waste residues generated in industrial production. Because PS and CS are not fully utilized, they have caused serious land occupation and resource waste. In this paper, PS and CS are used as auxiliary cementitious materials to study the modification mechanism of CS on PS and the synergistic mechanism of PS and CS in cement-based materials under different curing methods. First, CS can modify PS, weaken the retarding effect of phosphorus and fluorine elements remaining in PS on cement hydration, and promote the early hydration rate; secondly, CS can activate the volcanic ash activity of PS and reduce the adverse effects of the dilution effect. In addition, the generated hydration products can generate more SiO₂-Al₂O₃ gel with a low calcium-silicon ratio after carbonation and decalcification. Finally, the carbonated specimen shows better high-temperature mechanical properties and volume stability than the normally cured specimen, and the high-temperature strength and specimens volume initially rise and subsequently decline as temperature rises.

1. Introduction

According to statistics in recent years, China has become one of the countries with the world's largest production and consumption of OPC [1,2]. However, the OPC manufacturing process is associated with significant carbon emissions, contributing to severe environmental challenges [3–6]. According to relevant research statistics [7], the global cement production in 2022 reached 4.1 billion tons. Among them, China's cement production reached 2.1 billion tons, making it the world's largest cement producer. In 2021, the global carbon emissions generated by cement production were about 1.7 billion tons, causing serious damage to the ecological environment. Consequently, it is imperative to implement measures focused on minimizing the ecological footprint of the OPC sector [8]. In this context, many researchers have explored the combination of solid waste and carbonation solidification. Liu et al. [9] reviewed the latest progress in carbonation of industrial solid waste and concluded that carbonation of industrial solid waste can not only reduce the carbon content but also achieve the recycling of solid waste. Liu et al. [10] studied the use of waste concrete fine powder and

carbide slag as raw materials to prepare a new low-calcium CO₂ storage cementitious material. The results showed that the new low-calcium CO₂ storage cementitious material not only improves the utilization of industrial solid waste, but also can effectively reduce carbon emissions in the cement industry. Mehdizadeh et al. [11] studied the water carbonation of yellow phosphorus slag. The results showed that the carbonated yellow phosphorus slag not only sealed CO₂ but also increased its volcanic ash reactivity. Xu et al. [12] studied the carbonation of ladle slag and the results showed that ladle slag has good carbon sequestration capacity and can reduce the leaching concentration of heavy metal ions after carbonation. Xu et al. [13] studied the use of steel slag for carbon and zinc sequestration. The results showed that steel slag can not only seal carbon but also improve the timeliness of zinc sequestration. This process can store a large amount of carbon dioxide and offer a viable solution for repurposing industrial solid waste.

In environments rich in CO₂, the hydration products in cement [14–16], along with unhydrated clinker phases, react with CO₂, leading to the generation of CaCO₃ (CC), SiO₂ gel, and Al₂O₃ gel [17]. Cement itself has the natural ability to capture and store carbon. However, its overall carbon sequestration potential is limited by the high energy

* Corresponding authors.

E-mail addresses: yang_yixn@163.com (Y. Yang), jxliew@polyu.edu.hk (J.-X. Liew).

¹ Co-first authors: These authors contributed to the work equally and should be regarded as co-first authors.

Nomenclature

Abbreviations

PS	Phosphorus slag
CS	Carbide slag
OPC	Ordinary Portland Cement
CO ₂	Carbon dioxide
CC	CaCO ₃
AFt	Ettringite
C ₃ S	Tricalcium silicate
C ₃ A	Tricalcium aluminate
SCMs	Supplementary cementitious materials
CH	Calcium hydroxide
CBMs	Cement-based composites
NC	Normal curing
C	Carbonation curing
Hc	Hemicarboaluminate
Mc	Monocarboaluminate
AFm	Aluminum ferrite mono-sulfate
C ₂ S	Dicalcium silicate
C-S-H	Calcium silicate hydrate

consumption and carbon emissions involved in its production. Fortunately, several industrial waste by-products, such as soda residue, phosphorus slag (PS), and carbide slag (CS), exhibit high alkalinity and significant calcium content [18–20], providing an abundant calcium source and an alkaline environment conducive to hydration and carbonation. Therefore, utilizing industrial waste slag as a partial substitute for OPC and carbonation curing can mitigate the cement sector's adverse effects on the ecosystem.

PS refers to the solid byproduct generated during the smelting of phosphate ore [21]. The annual production of PS in both China and the United States exceeds 10 million tons [22,23]. The presence of amorphous SiO₂ and Al₂O₃ in PS is as high as 90 %, indicating its potential use as a supplementary cementitious materials (SCMs) [23–26]. Gao et al. [27] demonstrated that replacing a portion of cement with PS reduced harmful pores (>100 nm) and enhanced concrete microstructure and properties. Similarly, Zhang et al. [28] showed that in the advanced phase of hydration, the strength of a specimen containing 15 % or 30 % PS exceeded the strength of the OPC specimen. However, the residual phosphorus and fluorine in PS [29] can hinder early cement hydration, prolonging the induction period and leading to reduced early-stage strength [30]. This limitation may restrict its broader application in construction.

It is worth noting that a large amount of Ca²⁺ can convert soluble phosphorus and fluorine in PS into insoluble phosphate and fluoride [31], which helps to alleviate the adverse effects of impurities in PS on OPC hydration and strength development. Therefore, the use of materials with high Ca²⁺ content and high alkalinity (such as lime and CS) may be able to achieve the purpose of modifying PS. Mehdizadeh et al. [32] discussed the flow properties of PS slurry activated by a mixture of lime and alkali salts. The experiments demonstrated that the mechanical performance of the activated slurry improved, and the gel formation time was shortened. However, most construction lime is derived from

the calcination of limestone at 900°C, a process that adversely affects the environment. Calcium CS is the solid byproduct generated during industrial calcium carbide production. Its main component is CaO, which is similar to lime and has a high alkalinity. It can produce a large amount of Ca²⁺ after dissolving. Liu et al. [10] Examined the method of blending fine particles from recycled concrete with CS in different ratios, followed by calcination, to produce an innovative low-calcium cementitious material aimed at carbon fixation. The results showed that unhydrated cement clinker particles can react with carbon dioxide to form CC, enhancing the specimen's internal structure and thereby boosting its strength. Li et al. [33] used CS and lime to stimulate the pozzolanic activity of slag respectively. Under the same curing time, the mechanical properties of slag specimens stimulated by different activators were roughly the same. The higher pH value and calcium hydroxide (CH) content in CS can modify the PS, increase its initial hydration reaction rate to cement, stimulate the pozzolanic activity of the PS, and improve the matrix strength [34,35].

In summary, CS can be a good solid waste material for carbonation curing and can also be used as an auxiliary activator to achieve sustainable optimal utilization [36]. In addition, previous studies have focused on the activation of PS alone [37] or the addition of CS to improve the carbon sequestration capacity of cement-based materials (CBMs) [36]. There are few studies on the reaction mechanism of CS activating PS, the synergistic effect between CS and PS, and the combined effect of CS and PS on improving the carbon sequestration capacity of CBMs. This paper mainly discusses the mechanism through which CS can weaken the retarding effect of PS on the cement hydration process, and studies and explains the relevant mechanism by which the synergistic effect of CS and PS can not only improve the carbonation strength of CBMs, but also improve their CO₂ sequestration capacity.

The goal is to uncover the mechanisms of hydration and carbonation curing involving PS, CS, and CBMs, to enhance the utilization rates of these materials in cement-based composites and boost their carbon capture and storage capabilities. This study investigated the hydration mechanism, macroscopic properties, CO₂ absorption rate, high-temperature performance, phase composition, and microstructure of ternary composite materials of PS, CS, and cement; clarified the interplay between hydration and carbonation reactions in CBMs incorporating phosphorus and CS. The preliminary study examined how CS mitigates the adverse effects of PS on cement setting delay and explored the mechanism through which the synergy of these two materials enhances the CO₂ uptake potential of cement-based composites. This study focused on optimizing the role of PS as SCMs in cement blends and improving the mechanical properties, high-temperature performance, and carbon capture capabilities of PS and CS in cement composites.

2. Experimental design methods

2.1. Raw materials

The 42.5 OPC used in this study was produced by Huaxin Cement Co., Ltd., CS was produced in Changde, Hunan, quartz was produced in Shijiazhuang, Hebei, PS was produced in Yuxi, Yunnan, and fine aggregate was standard sand produced in Xiamen, Fujian. The oxide compositions of OPC, PS, CS, and quartz are listed in Table 1. The particle sizes of the different materials are shown in Fig. 1. Fig. 2 shows the XRD diffraction pattern of the raw material. According to the raw

Table 1

The materials consist of OPC, PS, CS, and quartz.

wt%	SiO ₂	Al ₂ O ₃	Fe ₂ O ₃	CaO	MgO	Na ₂ O	SO ₃	TiO ₂	P ₂ O ₅	Other
OPC	20.07	5.77	4.73	58.84	3.07	0.54	4.25	1.33	0.24	1.16
PS	42.28	3.25	4.65	42.71	2.18	0.39	0.42	0.36	2.41	1.35
CS	2.13	1.09	0.35	95.29	0.21	0.09	0.63	-	0.02	0.19
Quartz	98.75	0.92	0.04	0.02	0.07	-	0.02	0.03	0.01	0.14

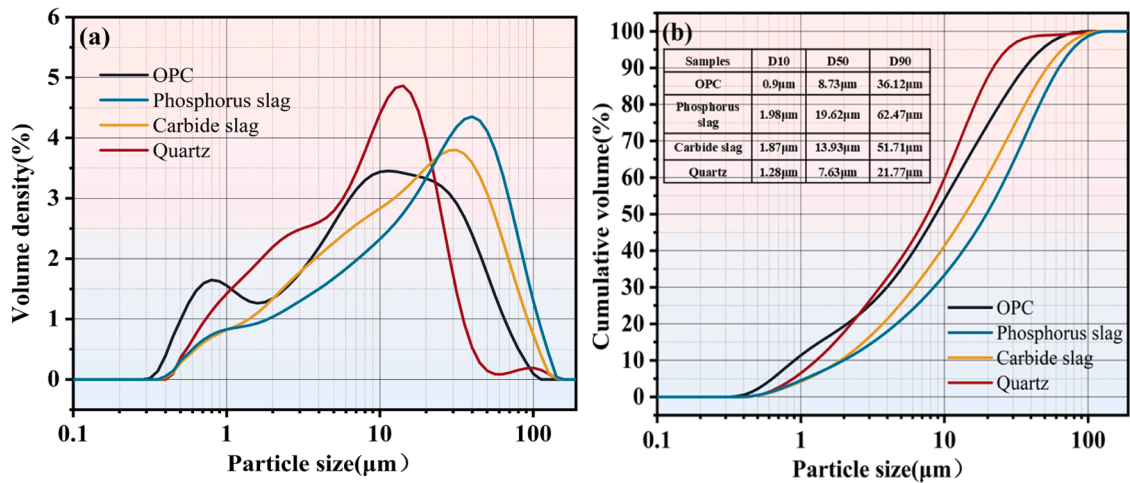


Fig. 1. Particle size curves of different materials.

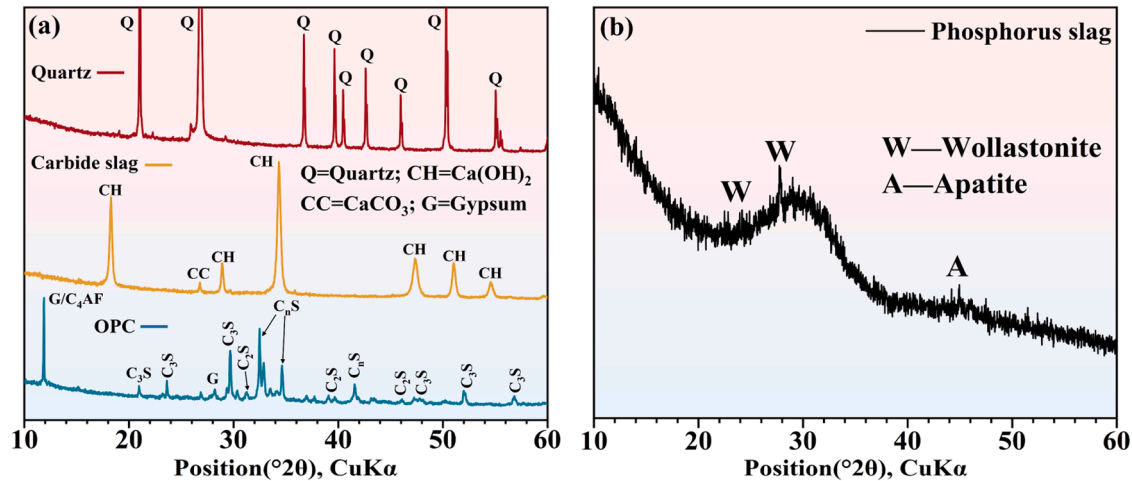


Fig. 2. (a) XRD results for quartz, CS, and OPC; (b) XRD results for PS.

Table 2

Design of the mix ratios for different specimens (Mass percentage).

Specimen code	OPC	PS	CS	Quartz	Water/ binder ratio
Q30	70			30	0.5
P30	70	30			
C30	70		30		
P10C20	70	10	20		
P15C30	55	15	30		
P20C40	40	20	40		

material particle size results (Fig. 1), keeping the particle size within a certain range can reduce errors affecting the specimen's hydration or carbonation effect. According to the XRF results (Table 1) and XRD results (Fig. 2) of the raw materials, CS mainly contains CaO and CH, and is an ideal solid waste material for CO₂ storage and carbonation curing; the inert material quartz mainly contains SiO₂, and its dilution and nucleation effects on cement can better improve the carbonation rate and promote the production of more hydration products. PS mainly contains SiO₂ and CaO, indicating that it has volcanic ash activity, but the P₂O₅ it contains will retard the setting of cement [34], and the high Ca²⁺ content in CS may reduce the soluble phosphorus content [31], which, thereby, weakens the retarding effect of PS on cement. It can be seen that the co-addition of phosphorus slag and carbide slag may have a

synergistic effect: on the one hand, it can improve the carbon sequestration capacity of the specimen, and on the other hand, carbide slag may activate the volcanic ash activity of phosphorus slag and produce additional hydration products. PS does not have obvious diffraction peaks, mainly dispersion peaks and "Broad peaks" [38].

2.2. Specimen production and curing conditions

The specimen mix ratio is detailed in Table 2. The substitution of quartz, PS, and CS for OPC is expressed as mass percentage. Four groups (Q30, P30, C30, and P10C20) were designed to study the effects of adding quartz, PS, CS, and the combination of PS and CS on the specimens under normal curing and carbonation curing conditions when the cement content was fixed at 70 %. In addition, three groups (P10C20, P15C30, and P20C40) were set up to study the effects of increasing the PS and CS contents on the specimens when the addition ratio of PS to CS was fixed at 1:2. The mortar-sand ratio is 1:2.5. Mix the materials according to the mixing proportions provided in Table 2 and then transfer them to a blender and mix them thoroughly. Finally, transfer the mixed slurry into a mold measuring 40 mm × 40 mm × 160 mm, wrap in plastic film to avoid air exposure, causing carbonation. The specimens are removed from the mold after one day.

For normal curing, the specimens are placed within a regulated setting with 65 % relative humidity and a temperature of 20°C. In contrast, during carbonation curing, the specimens are positioned in a

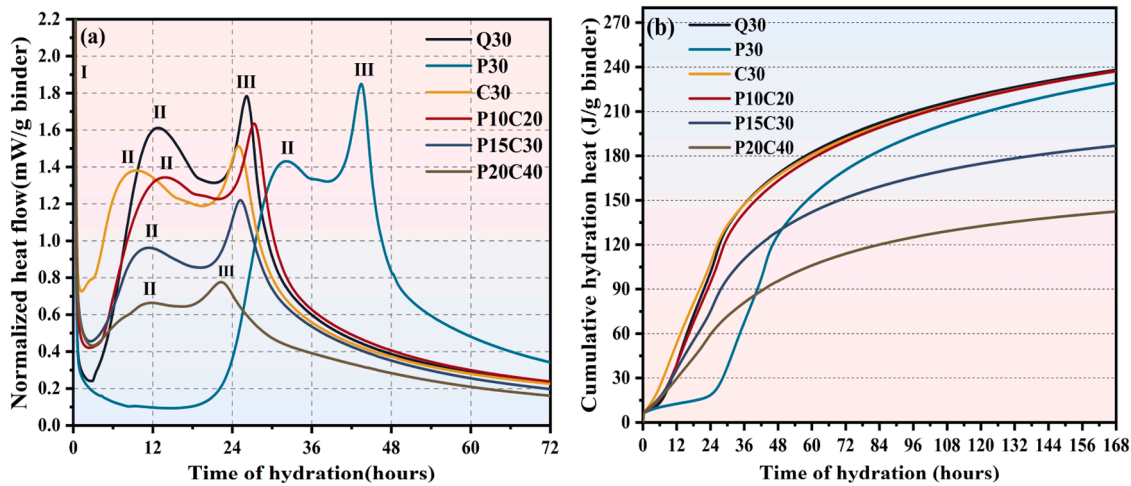


Fig. 3. Normalized heat flow curves of specimens with different ratios within 72 hours (a) and normalized cumulative heat release curves within 168 hours (b).

carbonation chamber kept at a relative humidity of 65 %, a temperature of 20°C, and a CO₂ concentration of 20 %. 20°C is to simulate the temperature of the specimen in most environments; at the same time, it can avoid the error caused by temperature under different curing methods. 60–70 % humidity is considered to be the optimal humidity range for cement-based carbonation curing [39]. The humidity of both normal curing and carbonation curing is controlled at 65 % to facilitate the comparison of the results of normal curing and carbonation curing. To differentiate between the curing conditions, specimens for normal curing are labeled as "NC," while those for carbonation curing are marked as "C".

2.3. Evaluation methods

2.3.1. Macro analysis methods

To assess the carbonation degree of mortar specimens at different ages, the principle of phenolphthalein indicator discoloration in the presence of alkali is employed to differentiate between carbonated and uncarbonated areas. The carbonation level was assessed by calculating the ratio of the colorless area of the specimen's cross-section to the overall sectional area.

The strength assessments are performed following ASTM C349 [40, 41]. After demolding, the compressive performance was tested with a universal testing apparatus.

For the high-temperature mechanical properties test, the specimens cured for 14 days were transferred to a muffle furnace and divided into three temperature ranges of 200°C, 600°C, and 900°C to simulate elevated thermal conditions. After reaching the predetermined temperature, they were kept warm for 1 hour and their residual strength was measured.

The volume stability of the specimens was evaluated using a thermal dilatometer (DIL16–50, China). The heating rate of the instrument is set to 5 °C/min, and the temperature range for the specimens during the experiment extends from 20°C to 1000°C.

2.3.2. Microanalysis methods

The hydration exothermic curve of the slurry at room temperature was analyzed using an isothermal calorimeter (TAM-air) to investigate the hydration reaction rate of different specimens. The testing duration was 7 days, with each specimen weighing 5 g. The pure slurry specimens were ground with agate, and the hydration process was halted using isopropanol and anhydrous ethanol solution [42].

The phase composition was analyzed by X-ray diffraction (XRD) using Rigaku SmartLab SE (Japan), the test angle was 5–90° and the scanning speed was 5°/min. Fourier transform infrared (FTIR)

spectroscopy was performed using Thermo Scientific Nicolet iS10 (USA) with a wavelength range of 400–4000 cm⁻¹, a resolution of 4 cm⁻¹, and 32 scans.

Thermogravimetric analysis (TGA) was performed using a HITACHI STA6000 (Japan) thermogravimeter with a heating rate of 5 °C/min, a minimum temperature of 50°C, and a maximum temperature of 1050°C. Use nitrogen (N₂) as protective gas.

The microstructure of the specimen cross-section was analyzed using a scanning electron microscope (Zeiss Sigma 300, Germany). In addition, the microstructure was further characterized using a transmission electron microscope (Thermo Fisher Talos F200X, USA). Finally, the porosity of the specimen was evaluated using an automated mercury intrusion instrument (Micromeritics Autopore V 9620, USA).

2.3.3. Carbon absorption calculation

Study the CO₂ absorption of the specimen in a carbon dioxide environment, the formula 1 was used in combination with the TGA data for calculation. This formula can eliminate some related errors in the experiment [43]. The CO₂ absorption rate is defined as the ratio of the mass of CO₂ absorbed by the specimen to the mass of specimen cement [44]. In Formula 1, A_{C600–900} represents the decomposition mass of the carbonation-cured specimen at 600–900°C, and A_{NC600–900} represents the decomposition mass of the normal-cured specimen at 600–900°C. The temperature range of 600–900°C is mainly based on the fact that carbonates (including calcium carbonate, magnesium carbonate, etc.) can be completely decomposed in this range, thereby eliminating the error caused by carbonation of the specimen by air or the small amount of carbonate it contains [45]. 600–900°C is the decomposition temperature of carbonates generated by reaction with CO₂ [45].

$$\text{CO}_2 \text{ uptake} = \frac{A_{C600-900} - A_{NC600-900}}{\text{mass of cement}} \quad (1)$$

3. Results

3.1. Hydration reaction

Fig. 3 illustrates the heat flow curve of different specimens at 72 hours (a) and the cumulative heat release curves at 168 hours (b).

In specimens, P15C30 and P20C40, the hydration reaction process of the binder was impacted to some degree, and the degree of reaction showed a decreasing trend, likely due to a dilution effect as increased proportions of PS and CS reducing hydration reaction's exothermic peak [43,46]. Moreover, incorporating PS notably prolongs the induction phase in the P30 specimen when compared to other specimens. This observation is consistent with Chen's research [29], which indicates that

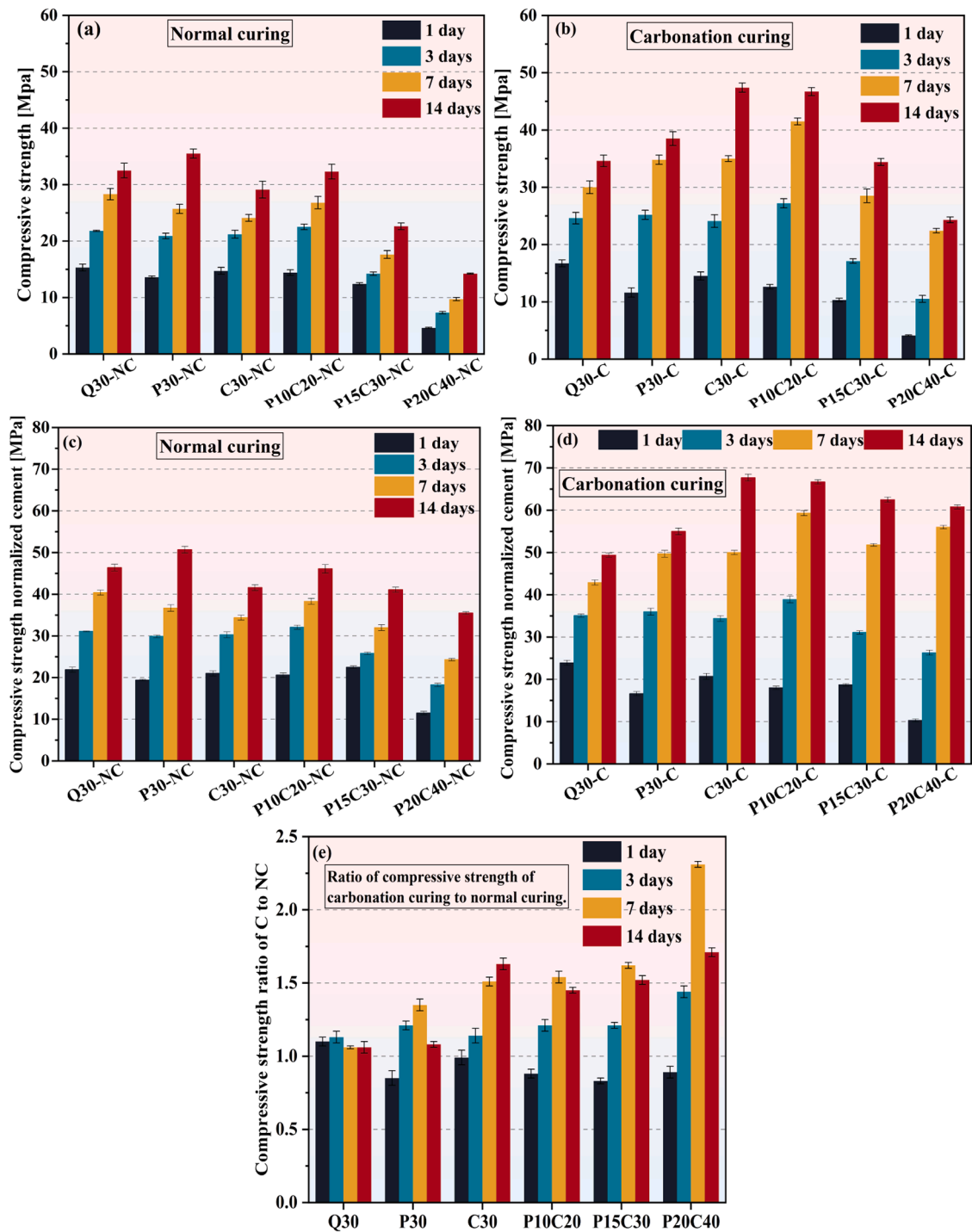


Fig. 4. (a) Compressive strength of specimens at different ages under normal curing; (b) Compressive strength of specimens at different ages under carbonation curing; (c) Normalized cement strength of specimens under normal curing at different ages; (d) Normalized cement strength of specimens under carbonation curing at different ages; (e) Ratio of carbonation-cured strength to normal-cured strength of specimens at different ages. (NC stands for normal curing, C stands for carbonation curing).

the residual phosphorus present in PS can inhibit the hydration process of cement.

Fig. 3a illustrates that the induction period for the ternary binder composed of OPC, PS, and CS is significantly shorter compared to the binary binder made from OPC and PS. This phenomenon can be explained by several factors: (1) CS activates the activity of PS volcanic ash, generates more hydrated gel, refines the matrix pore size, and improves mechanical properties [27,28,35]. (2) The abundant Ca^{2+} released from CS hydration reacts with phosphorus and fluorine in PS,

forming insoluble phosphates and fluorides, which reduces the blocking effects of phosphorus and fluorine on hydration [31].

As shown in Fig. 3b, the addition of quartz to the Q30 specimen promotes the clinker hydration; making the overall accumulated heat of the Q30 specimen in 7 days higher than that of other specimens [43,46]. Interestingly, the exothermic latent period of the P10C20 specimen is earlier than that of the P30 specimen. On the one hand, the high pH value and calcium oxide content of the CS weaken the effects of impurities such as phosphorus and fluorine [31], and the CS modifies the PS

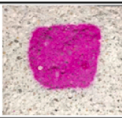
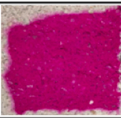
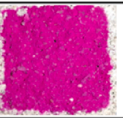
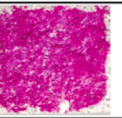
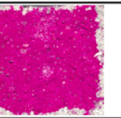
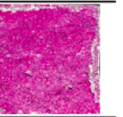
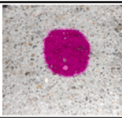
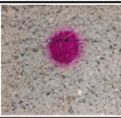

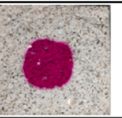
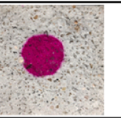

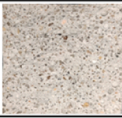

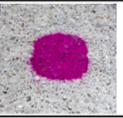
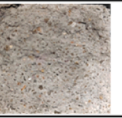

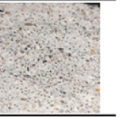




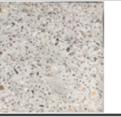
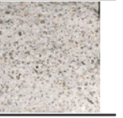
	Q30-C	P30-C	C30-C	P10C20-C	P15C30-C	P20C40-C
1 day						
Carbonation degree	70.1%	20.2%	13.5%	21.2%	22.7%	7.4%
3 days						
Carbonation degree	85.8%	92.1%	69.8%	83.7%	88.6%	82.8%
7 days						
Carbonation degree	100%	100%	82.7%	100%	100%	100%
14 days						
Carbonation degree	100%	100%	100%	100%	100%	100%

Fig. 5. phenolphthalein reagent was utilized to measure the carbonation area of the specimens at different carbonation curing periods.

and promotes the hydration of the slurry; On the other hand, the CS reacts with the PS to increase the heat released from the slurry [27]. The total heat output from the hydration of P15C30 and P20C40 specimens decreases in sequence [43,46,47]. This trend is because the adverse effects of dilution influence dominate, resulting in a relatively low cumulative heat release.

3.2. Mechanical properties

The strength of the specimens under different curing conditions is shown in Fig. 4a and b; the strength of the specimens normalized to cement under the two curing conditions is shown in Fig. 4c and d; Fig. 4e shows the compressive strength ratio under the two curing conditions.

The data in Fig. 4a indicates that, at the same level of cement replacement, the P30-NC specimen shows lower early compressive strength; however, its strength at 14 days exceeds that of all other mixtures. This phenomenon occurs because CH activates the pozzolanic activity of the PS, leading to the formation of additional calcium silicate hydrate gel [48]. After one day of normal curing, the strength of the P10C20-NC specimen is lower than that of the C30-NC specimen. This can be attributed to the presence of PS in the P10C20-NC specimen, where residual phosphorus hinders early cement hydration, leading to reduced initial strength [29,49]. CH converts the phosphorus in PS into insoluble hydroxyapatite and calcium phosphate. These compounds adhere to the surfaces of unhydrated particles, impeding early hydration and causing reduced initial strength [35,50]. However, after the initial stage of normal curing, the strength of the specimen containing only CS was lower than that of the P10C20-NC specimen. This discrepancy may be attributed to the activation of the pozzolanic activity of PS by CS, which facilitates the generation of calcium silicate hydrate gel, thereby enhancing the paste strength [27,35,51]. In addition, the strength increase brought about by the pozzolanic reaction between PS and CS cannot compensate for the adverse effects of the decline of cement content, causing the gradual reduction in the strength of P15C30-NC and P20C40-NC specimens with the increase of the replacement amount.

As illustrated in Fig. 4b, the Q30-C specimen exhibits higher strength at 1 day compared to other groups. This could result from the nucleation impact of quartz accelerating the carbonation of the specimen [43,46]. At 14 days, the C30-C specimen reaches the highest strength among all

groups, likely because its higher CS content increases CH levels. In an environment rich in carbon dioxide, CH readily carbonates into CC, which fills pores and refines paste structure, enhancing overall strength [52]. Comparing Q30-C with P10C20-C, the Q30-C specimen shows slightly higher strength at 1 and 3 days, but the P10C20-C specimen surpasses it at 7 and 14 days. Possible reasons for this are: (1) The pozzolanic reaction between PS and CS generates more hydrated gel, which is then carbonated and decalcified to generate CC and silica gel, which refines the pore size [17,27,53]. (2) CS increases CH in the matrix, producing more CaCO_3 during carbonation and thereby boosting specimen strength [36,52]. Across all ages, the P10C20-C specimen exhibits higher strength than the P30-C specimen, likely due to the increased CH from CS, which produces additional CC crystals in carbonation, enhancing strength [36,52].

Fig. 4c shows that in the first three ages of normal curing, the strength of the P10C20-NC specimen was slightly superior to that of the P30-NC specimen. This was mainly because CH in the CS reduced the influence of impurities on the hydration of clinker and producing a pozzolanic reaction with the PS [27,35], which promotes the growth of early strength of specimens.

Fig. 4e shows that the strength of the specimens containing CS continues to increase in the subsequent stage of carbonation, and the strength is superior to the normal curing strength. This phenomenon is ascribed to the reaction of CH with carbon dioxide in CS to form CC, which refines the matrix pores. However, by adding PS, the strength ratio of the specimen also decreases significantly. This decrease was mainly due to the competitive interaction between the pozzolanic reaction of PS and the carbonation reaction of PS. In addition, the P20C40 specimen has higher strength performance after carbonation curing, indicating that the effect of carbonation curing is significantly better than normal curing. Because of the elevated levels of CS, the matrix contains a high amount of CH, which is conducive to the reaction with CO_2 . The products of the carbonation reaction can effectively improve the micropore structure of the specimen, resulting in a denser structure and considerably enhancing the mechanical characteristics of the specimen [46,54].

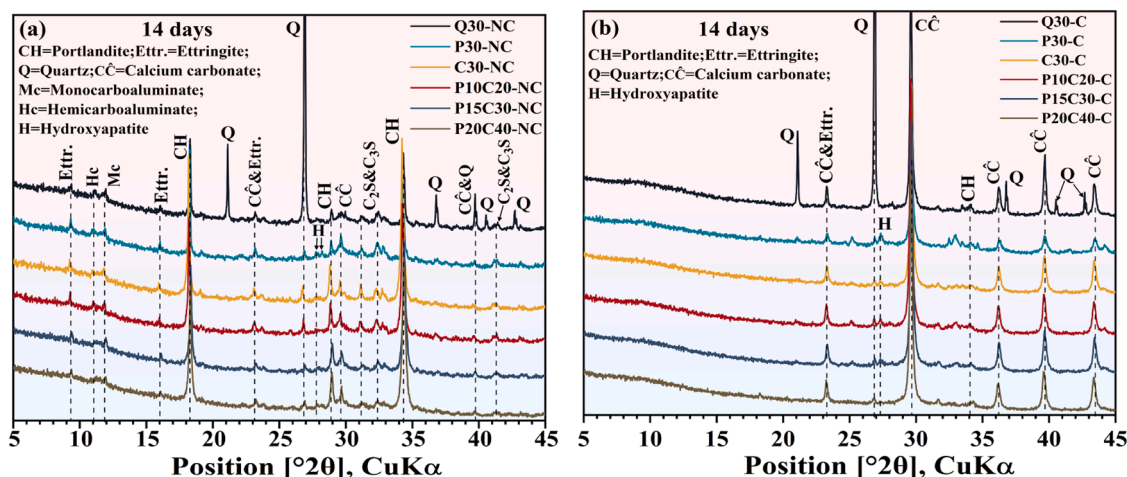


Fig. 6. XRD diffraction patterns of specimens under various curing conditions.

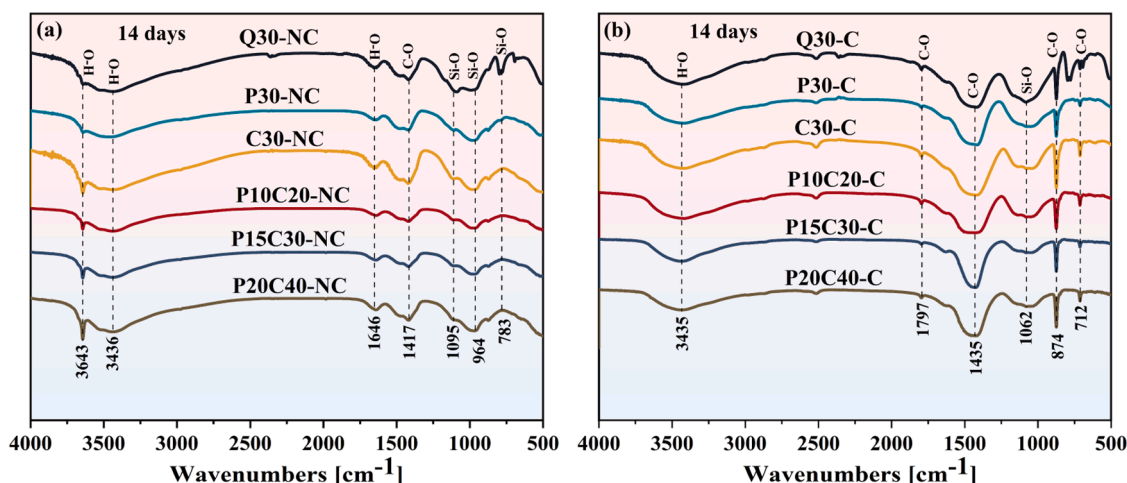


Fig. 7. FTIR results of specimens under different curing conditions.

3.3. Carbonation level

The carbonation levels of the specimens at different carbonation phases are referred to in Fig. 5. Notably, after 1 day, the Q30-C specimen exhibited the highest carbonation area among all specimens, reaching 70.1 %. This result is attributed to the nucleation role of quartz during the process of carbonation, accelerating the rapid spreading of CO₂ in the specimen [43,55]. At 3 days, the carbonation area of the P30-C specimen increased the most, which was because of the pozzolanic reaction between the PS and CH in the specimen, because it reduced the CH content in the specimen. In addition, CH also undergoes a carbonation reaction with CO₂, and the two reactions consume CH at the same time, resulting in the expansion of its carbonation area [48,56]. Since the specimen contains more CS, the CH content of the specimen rises. The carbonation level of the C30-C specimen increases the slowest. However, P15C30-C and P20C40-C specimens were completely carbonated in 7 days, and their carbonation levels were higher than those of the C30-C specimens. The possible reasons for this result are: (1) the introduction of PS and CS has a dilution impact on cement. (2) CS activates the volcanic ash activity of PS, and PS and CS undergo a pozzolanic reaction, which accelerates the consumption of CH [27,35, 51].

3.4. Reaction products

The XRD spectrum of the specimen at 14 days of curing is shown in Fig. 6; the FTIR spectrum of the specimen at an age of curing for 14 days is shown in Fig. 7. As shown in Fig. 6a and b, under different curing conditions, the diffraction peak of hydroxyapatite ($\text{Ca}_{10}(\text{PO}_4)_6(\text{OH})_2$) (around $2\theta = 28^\circ$) was detected in all specimens with added PS [57]. This is attributed to the reaction between P_2O_5 in the PS and CH [35,50]. At the end of normal curing, the diffraction features of calcium sulfonate were detected in all specimens (see Fig. 6a). This phenomenon may be caused by the reaction of C_3A in the slurry with sulfate [58]. After 14 days of normal curing, diffraction features of hemicarboaluminate (Hc) and monocarboaluminate (Mc) were detected in all specimens. This may be because the sulfate in the specimen was consumed early, resulting in insufficient sulfate content later, leading to the conversion of Aft to Hc and Mc [47,59,60]. As shown in Fig. 6b, after carbonation curing, the diffraction features of ettringite, Hc, C_3S , C_2S , and CH in all specimens disappeared and turned into more obvious diffraction peaks of CC. The reason for this result may be that ettringite reacts with CO_2 and carbonates to produce CC and Al_2O_3 gel [17]. Additionally, CH, C_3S , and C_2S can also undergo carbonation reactions to generate CC [17,43,61].

As shown in Fig. 7a and b, The vibrations of CO_3^{2-} are located at approximately 1431 cm^{-1} , 1417 cm^{-1} , 874 cm^{-1} , and 712 cm^{-1} [43]. Additionally, the stretching vibration peak of CO_3^{2-} occurs at approximately 1795 cm^{-1} [62]. The O-H stretching vibration peaks for CH are

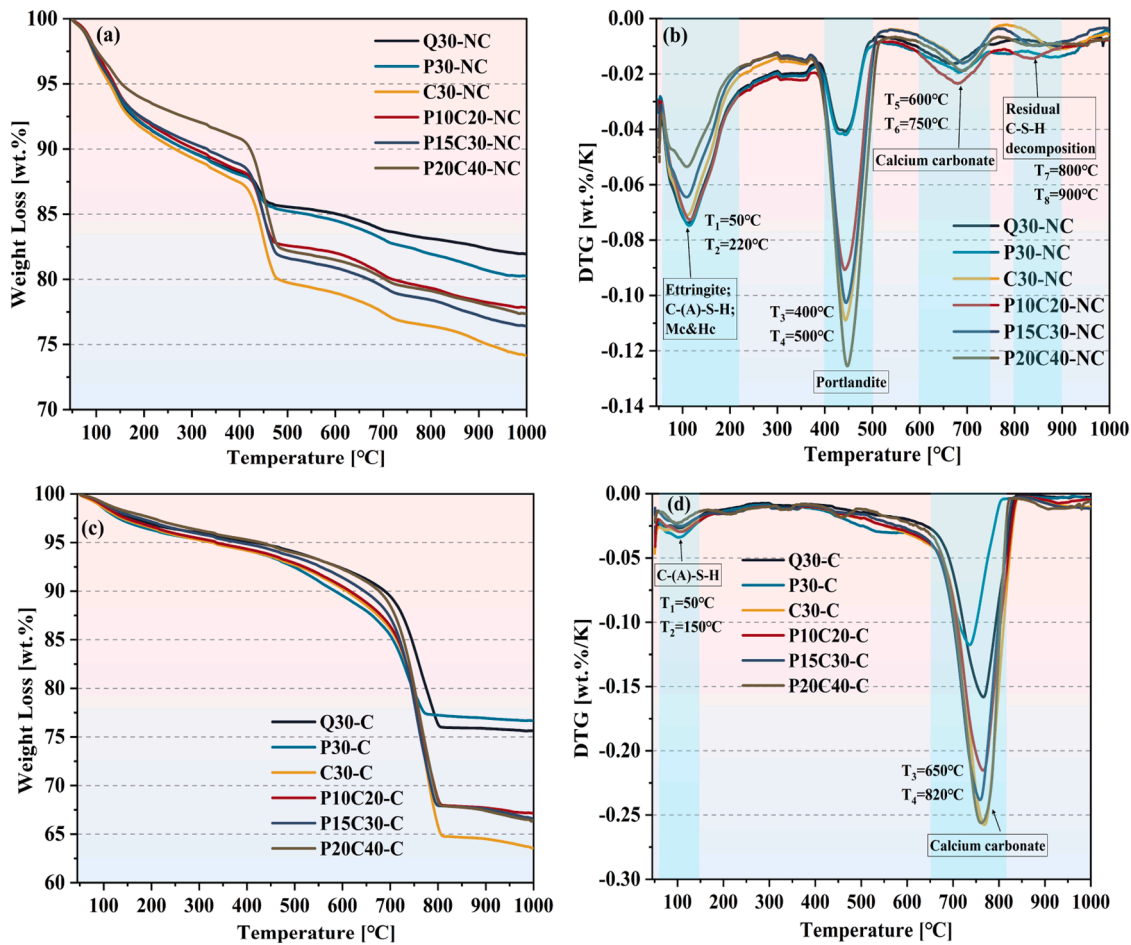


Fig. 8. TGA and DTG of specimens under different curing conditions at 14 days.

located around 3646 cm^{-1} and 3643 cm^{-1} [63].

The broad peaks appearing at wavelengths of 3645 cm^{-1} and 3643 cm^{-1} may be the stretching vibrations of the O-H bonds in CH (see Fig. 7a). The peaks in the P20C40 specimen were especially strong, which may be due to the large amount of CS added to this group, resulting in a high content of CH in the paste. As shown in Fig. 7b, the O-H stretching vibration peak of CH disappeared significantly, because the carbonation reaction consumes the CH content.

Fig. 7a and b clearly show that for all specimens, the absorption peaks at 1646 cm^{-1} and 964 cm^{-1} disappear, while the peak at 1062 cm^{-1} is enhanced because of the carbonation reaction with CO₂. In a CO₂-abundant setting, calcium silicate hydrate gel undergoes a carbonation reaction with CO₂, leading to its gradual consumption and explaining this observed phenomenon. Concurrently, the reaction between calcium silicate hydrate gel and CO₂ promotes the generation of SiO₂ gel [17,56], resulting in the detection of a shifted Si-O absorption peak at 1062 cm^{-1} after carbonation [46].

3.5. TG thermal analysis

Fig. 8 shows the TGA and DTG data of the specimens at 14 days under various curing conditions.

As shown in Fig. 8b, the weak endothermic peak at $800\text{--}900^\circ\text{C}$ may be due to the thermal decomposition of the residual C-S-H internal long chains and the transformation into other non-structural and amorphous gels [64]. After 14 days of normal curing, the specimen with CS added alone showed a higher endothermic peak at around 450°C than the specimen with quartz added alone. At about 100°C , owing to the pozzolanic activity of PS, more hydrated gel is generated, resulting in

Table 3

CH content and CO₂ uptake (14 days).

	calcium hydroxide content (wt%)	carbon dioxide uptake (wt%)
Q30-NC	13.37	/
P30-NC	12.56	/
C30-NC	38.85	/
P10C20-NC	28.77	/
P15C30-NC	36.39	/
P20C40-NC	43.21	/
Q30-C	/	15.7
P30-C	/	14.9
C30-C	/	41.6
P10C20-C	/	35.2
P15C30-C	/	38.8
P20C40-C	/	41.2

the weight loss peak of the specimen with only PS introduced being slightly exceeding that of the specimen with only quartz introduced [51]. In addition, the endothermic peaks of P20C40-C and C30-C specimens are the highest at around 750°C , which is due to the incorporation of CS in the specimens, which increases the content of CH in the matrix and generates more CC after carbonation.

The weight loss of the specimens at $50\text{--}1050^\circ\text{C}$ was obtained by calculating from the TGA curve; the CC content of the specimen with only PS is slightly lower than that of the quartz introduced specimen (refer to Table 3). This difference is mainly caused by two factors: first, the pozzolanic reaction involving PS consumes part of the available CH [35]; second, carbonation products create a coating on the surfaces of

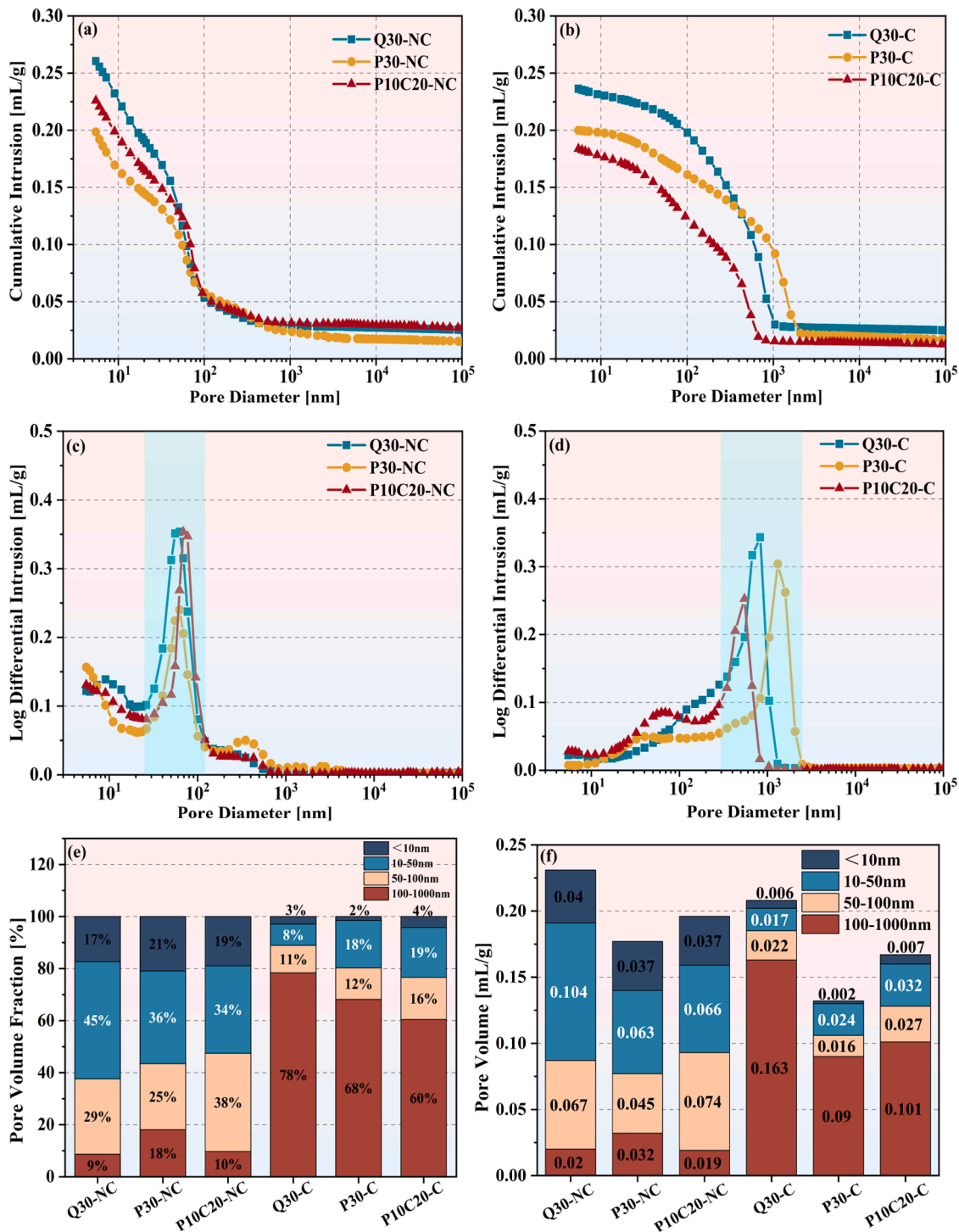


Fig. 9. (a) and (c) are the MIP for the specimens cured for 14 days.; (b) and (d) are the MIP of the specimens carbonated for 14 days; (e) and (f) respectively show the pore volume distribution after curing for 14 days.

unreacted cement clinker and PS particles, which limits their interaction with water [65]. Consequently, this reduction in water contact results in decreased formation of CH, leading to a lower CC content in the P30-C specimen.

3.6. Pores and pore structure analysis

Fig. 9a-d indicate the pore size range of specimens under carbonation curing and normal curing conditions for 14 days; Fig. 9e and f show the pore size percentages in different ranges of specimens under different

curing conditions. The size and distribution of specimen pores can have a significant impact on specimen performance. According to relevant research by Chen et al. [66], pores in different pore size ranges have different effects on specimen performance and durability [67]. Based on the test results, the pore sizes are divided into different categories: gel capillary pores (less than 10 nanometers), fine capillary pores (10 nanometers to 50 nanometers), medium capillary pores (50 nanometers to 100 nanometers), and large capillary pores (100 nanometers to 1000 nanometers) [68–70]. Pores with a diameter of less than 50 nanometers are classified as micropores, while pores larger than 50 nanometers are

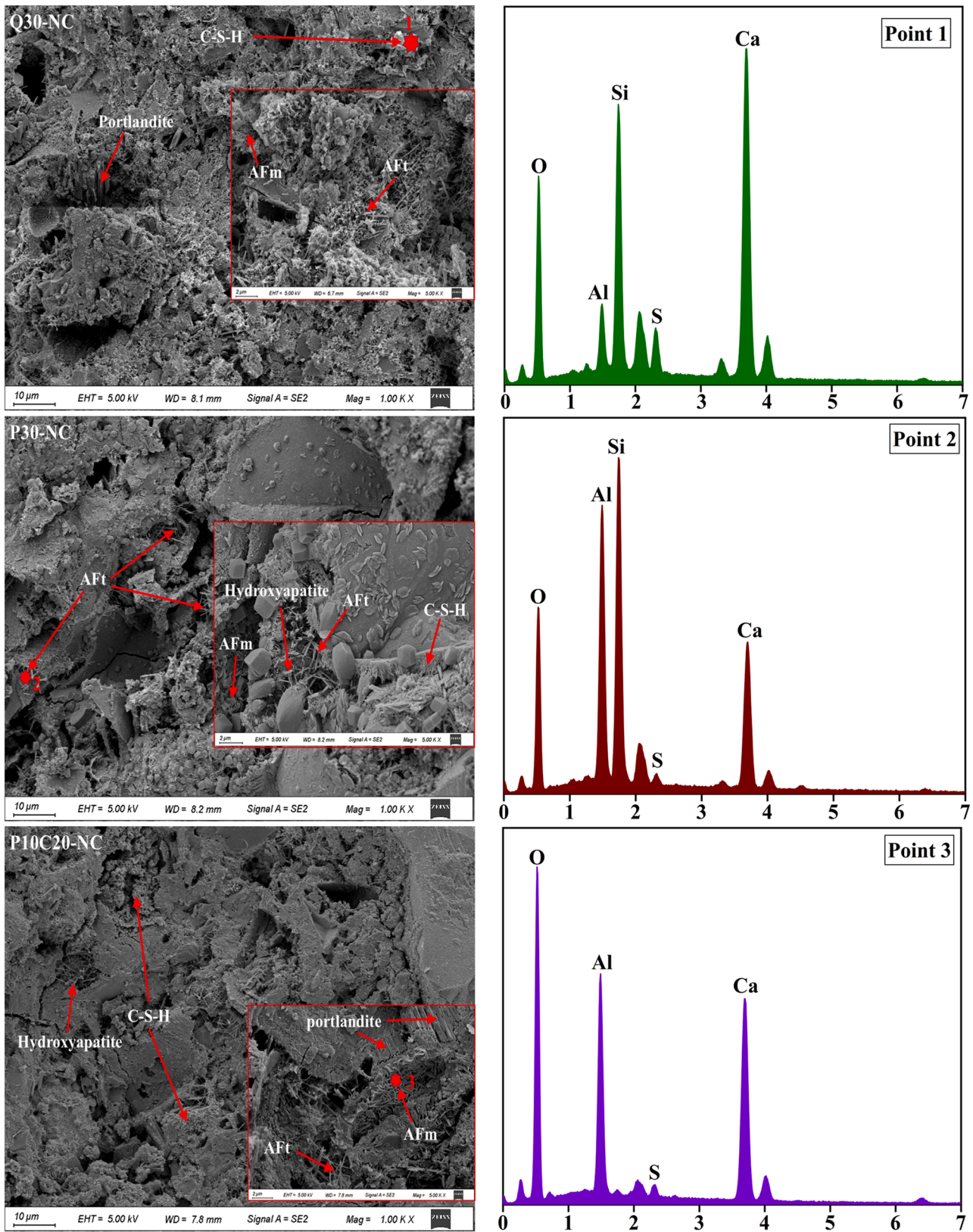


Fig. 10. SEM images and EDS of specimens after 14 days under different curing conditions.

called macropores. The higher the micropore density, the tighter the pore structure, which generally leads to increased strength [71].

As shown in Fig. 9a-f, the average pore size of the carbonated

specimens increased compared to the normally cured specimens, but the total pore volume decreased. This result is consistent with previous studies [41]. This is a result of two factors: (1) A large number of CC

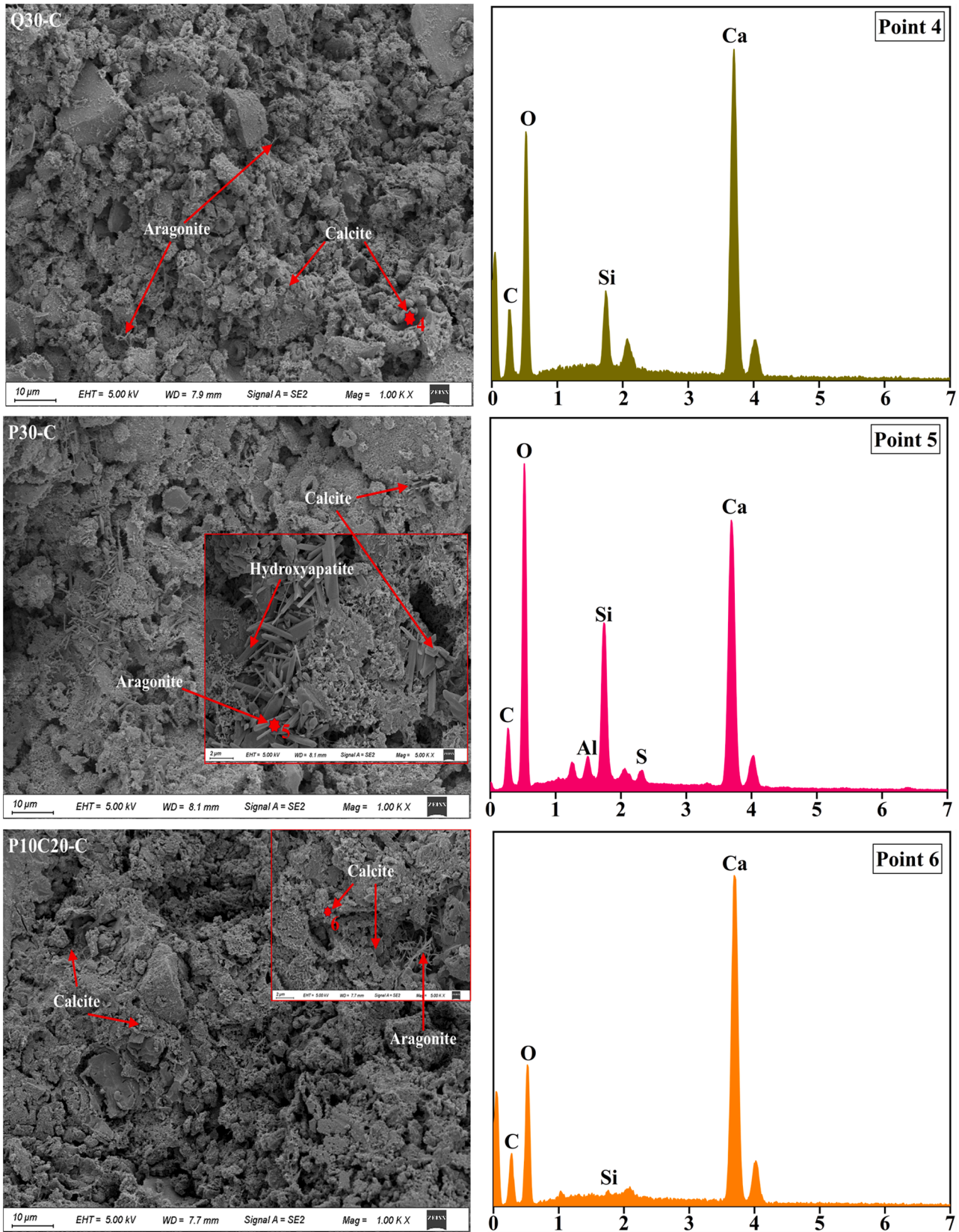


Fig. 10. (continued).

crystals are produced after carbonation, and the CC crystals fill the small pores of the paste, generating pore pressure [53], resulting in the transformation of small pores into larger ones. (2) Because of the

decalcification of hydration products [72], smaller pores are filled, resulting in a denser microstructure.

As illustrated in Fig. 9c and e, under normal curing conditions, PS has

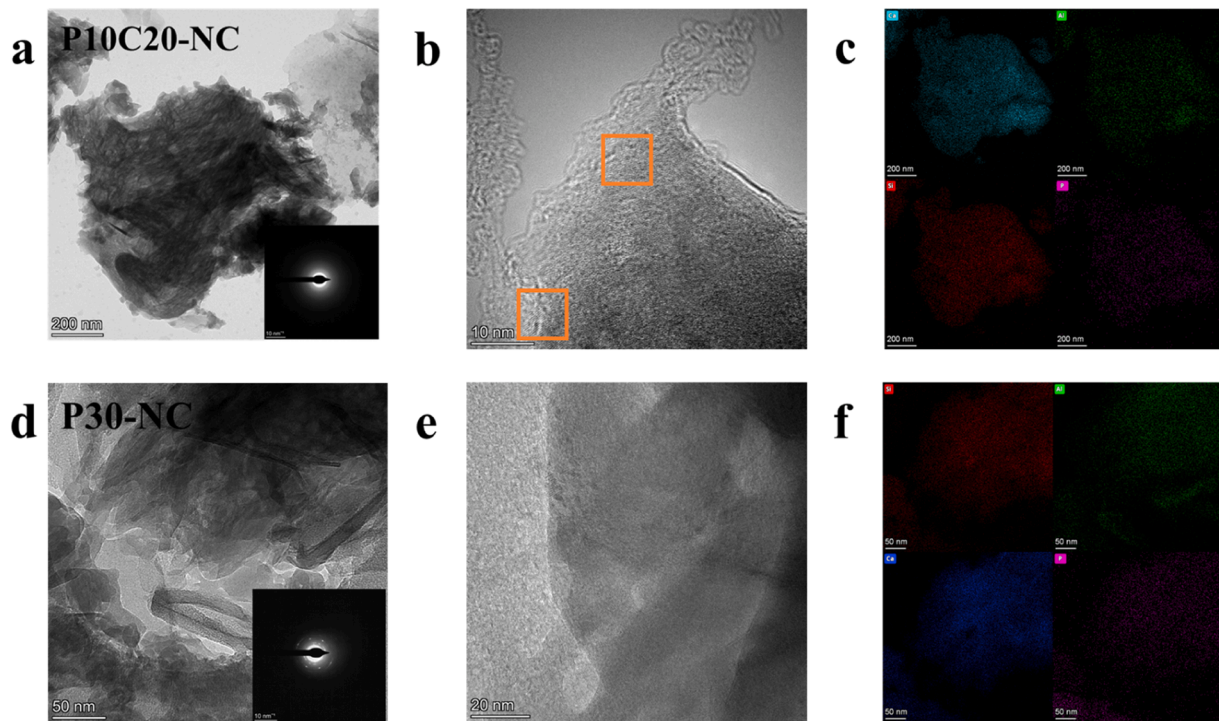


Fig. 11. (a)-(f) TEM and EDS of specimens after 14 days of normal curing.

pozzolanic activity [27,35], forming a more hydrated gel, thereby refining the matrix pore structure [73]; the gel capillary porosity of the P30-NC specimen is superior to that of the Q30-NC specimen.

It can be seen from Fig. 9d and e that under carbonation curing conditions, since quartz is an inert material and cannot react with CO₂, the proportion of macropores in the Q30-C specimen is greater than that observed in the P30-C and P10C20-C specimens.

3.7. Microscopic morphology characterization

Fig. 10 shows the SEM images and EDS of the specimens after curing for 14 days. The morphology of C-S-H is flocculent [74], AFt and AFm are needle-shaped and flake-shaped, respectively [75], while calcite and fibrous aragonite are rhombohedral blocks and long strips [75]. Each specimen exhibited different compositions and micromorphologies under varying curing conditions. Under normal curing conditions, the specimens contained AFt, calcium silicate hydrate gel, and CH [41,43,55,76]. In contrast, carbonation curing conditions revealed the presence of calcite and fibrous aragonite, aligning with findings from XRD, TGA, and FTIR analyses. Research has indicated [46] that calcite crystals possess greater crystallinity, molar volume, and hardness in comparison to CH [52]. The precipitation of calcite can effectively occupy voids within the material, thereby enhancing the specimen's strength. Furthermore, hydroxyapatite was identified in all specimens containing PS [57], corroborating the results obtained from XRD studies.

Fig. 11a-f show the TEM images of P10C20-NC and P30-NC specimens after 14 days, and Fig. 12a-l show the TEM images of Q30-C, P10C20-C and P30-C specimens after 14 days. In Figs. 11a and 11d, a large amount of fibrous gel can be observed in the matrix. According to the comprehensive analysis of EDS and SAED results, the fibrous gel is mainly calcium silicate hydrate gel. In addition, the fibrous gel was interwoven to form a dense cementation structure, which laid the foundation for the formation and development of matrix strength [38]. By comparing Fig. 11a and d, less fibrous calcium silicate hydrate gel was observed in the P10C20-NC specimen. This is because the CS dilutes the PS content, resulting in less PS participating in the pozzolanic reaction. Fig. 11b and e show that a discontinuous lattice can be observed

in the P10C20-NC specimen, which is due to the pozzolanic reaction of part of the CS with the PS to form an amorphous phase hydrated gel. Fig. 11c and f show that since phosphorus can be fixed by calcium silicate hydrate gel, the phosphorus in the PS is evenly distributed in the gel, so the delayed impact of phosphorus on hydration in the later stage is eliminated [77].

At the final stage of carbonation, the Q30, P10C20-C, and P30-C specimens are mainly composed of blended and interwoven CaCO₃ and SiO₂-Al₂O₃ gels. From the SAED and lattice results in Fig. 12, a large number of crystalline phases appear in the carbonated specimen, and the lattice spacing is 0.298 nm, 0.280 nm, and 0.261 nm, respectively, which show different diffraction halos. The lattice size may be related to the nucleation of CC.

3.8. High-temperature performance

Fig. 13a and b show the strength of specimens calcined at different temperatures for 1 hour at 14 days under different curing conditions. Fig. 13c and d show the strength of the specimens normalized at 20°C. In addition, Fig. 14a and b show the linear expansion rate for specimens within a temperature range of 25°C to 1000°C. Fig. 14c and d show the high-temperature expansion ratios of the specimens.

As illustrated in Fig. 13a and b, all specimens, except the C30-NC group, exhibit a compressive strength trend after high-temperature calcination that initially rises and then declines as the temperature increases [78]. Several factors may account for this behavior: (1) The internal autoclave effect is likely a significant contributor [79,80]. When the temperature of the specimen surpasses 100°C, the water present in the pores converts to steam and diffuses outward. However, steam trapped within closed pores cannot escape, leading to the accumulation of internal stress, which ultimately enhances the strength of the specimen [78]. (2) Since the unreacted particles continue to undergo hydration reaction in the presence of elevated temperatures and pressures, the strength of the specimen increases at 200°C [47]. Since the C30-NC specimen has more interconnected pores, which allow water vapor to escape, it cannot generate internal stress, causing a decline in the strength of the specimen. Due to the volcanic reaction of PS, more

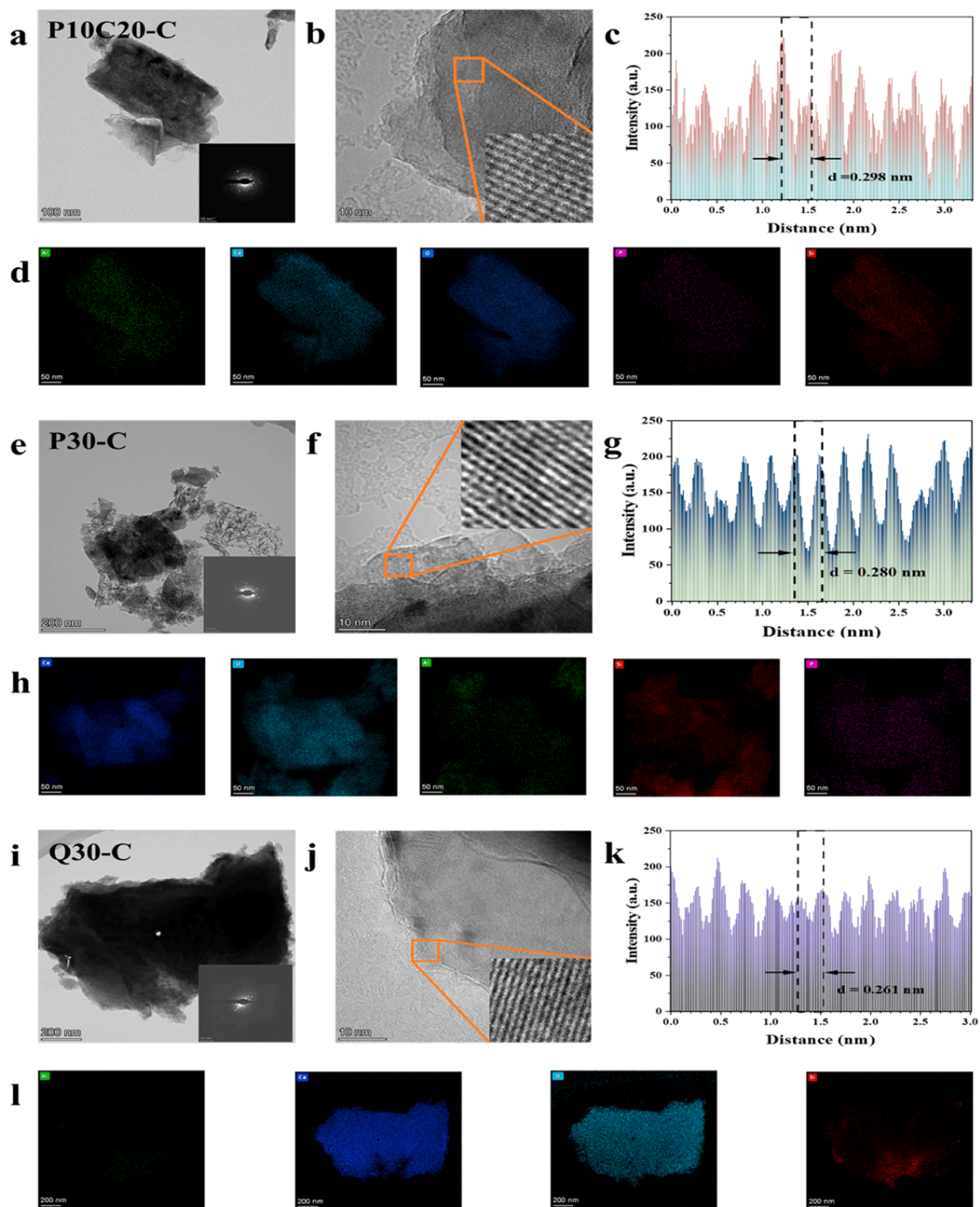


Fig. 12. (a)–(l) TEM, EDS, and lattice spacing of specimens cured by carbonation for 14 days.

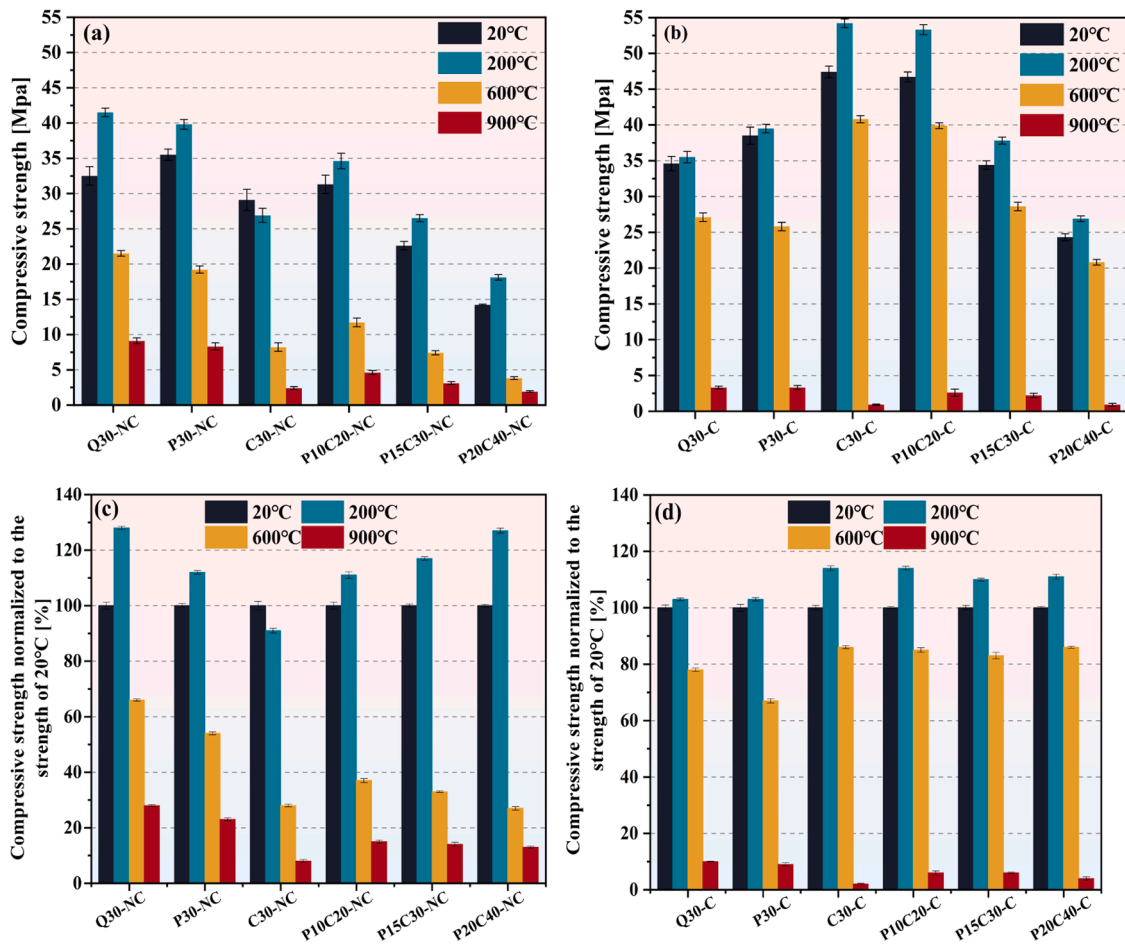


Fig. 13. (a)-(b) represent the strength of specimens with different curing conditions at different temperatures; (c)-(d) show the normalized strength of specimens with different curing conditions at 20°C.

Calcium silicate hydrate gel is generated, which is prone to decomposition between 50°C and 200°C, resulting in the strength of the P30-NC specimen being lower than that of the Q30-NC specimen [41]. At 600°C, the strength of all specimens decreased, but the strength of specimens under normal curing decreased more than that of the specimens cured by carbonation. The reason for this result is not only the hydration products decomposition but also the CH decomposition. As shown in Fig. 13b and d, at 200°C, the strength of all carbonation-cured specimens increased. However, after the temperature rose to 500°C, the strength of the specimens began to decrease, which was mainly due to the volatilization of crystal water and volume expansion [41]. At 900°C, the strength of all specimens decreased, which was attributed to the degradation of CC.

As illustrated in Fig. 14a and b, the porosity is increased due to the increased presence of macropores in the carbonated specimens (see Fig. 9e), resulting in a higher thermal expansion coefficient compared with the normally cured specimens; thus, the linear expansion of the carbonated specimens is superior to that of the normal curing specimens [81]. The observation that specimens with a higher thermal expansion coefficient exhibit greater linear expansion at a given temperature aligns with findings from previous studies [41]. Between 100°C and 650°C, all specimens exhibit irregular linear expansion, irrespective of the curing method. This irregularity may be due to the differing thermal expansion behaviors of quartz along various crystallographic directions. Conversely, between 650°C and 1000°C, specimens demonstrate irregular contraction, likely resulting from the decomposition of carbonation products at elevated temperatures [82].

As illustrated in Fig. 14c and d, shrinkage cracks appeared in all

specimens at 100°C as a result of the vaporization of unbound water in the specimens, shrinkage, and decomposition of hydration products [83, 84].

4. Discussion

Fig. 15 illustrates the carbonation mechanism of the ternary binder composed of PS, CS, and OPC.

In this experiment, specimens containing quartz were used as the control group, and conventional curing and carbonation curing were performed on each type of specimen. A comparative analysis of the two curing conditions revealed that the conclusion of the carbonation process coincided with the cessation of the hydration process, suggesting that the carbonation procedure takes place at a quicker pace than hydration. Furthermore, it was observed that increased alkalinity inhibits paste hydration, corroborating findings from prior studies [43,46,85].

Comparing specimens with PS or CS added separately to specimens with both materials added simultaneously, it was found that PS and CS had a synergistic effect in the hydration and carbonation stages. This interaction significantly influences both reactions. During the hydration stage, CS can reduce the phosphorus and fluorine content in the PS, thereby achieving the purpose of modifying the PS, weakening the adverse effect of the PS on the clinker hydration process, and promoting the growth of the initial strength of the matrix. In the carbonation stage, the combined effect of PS and CS not only boosts the subsequent strength of the specimens but also enhances their ability to capture and store carbon.

PS and CS as SCMs show broad prospects in practical application

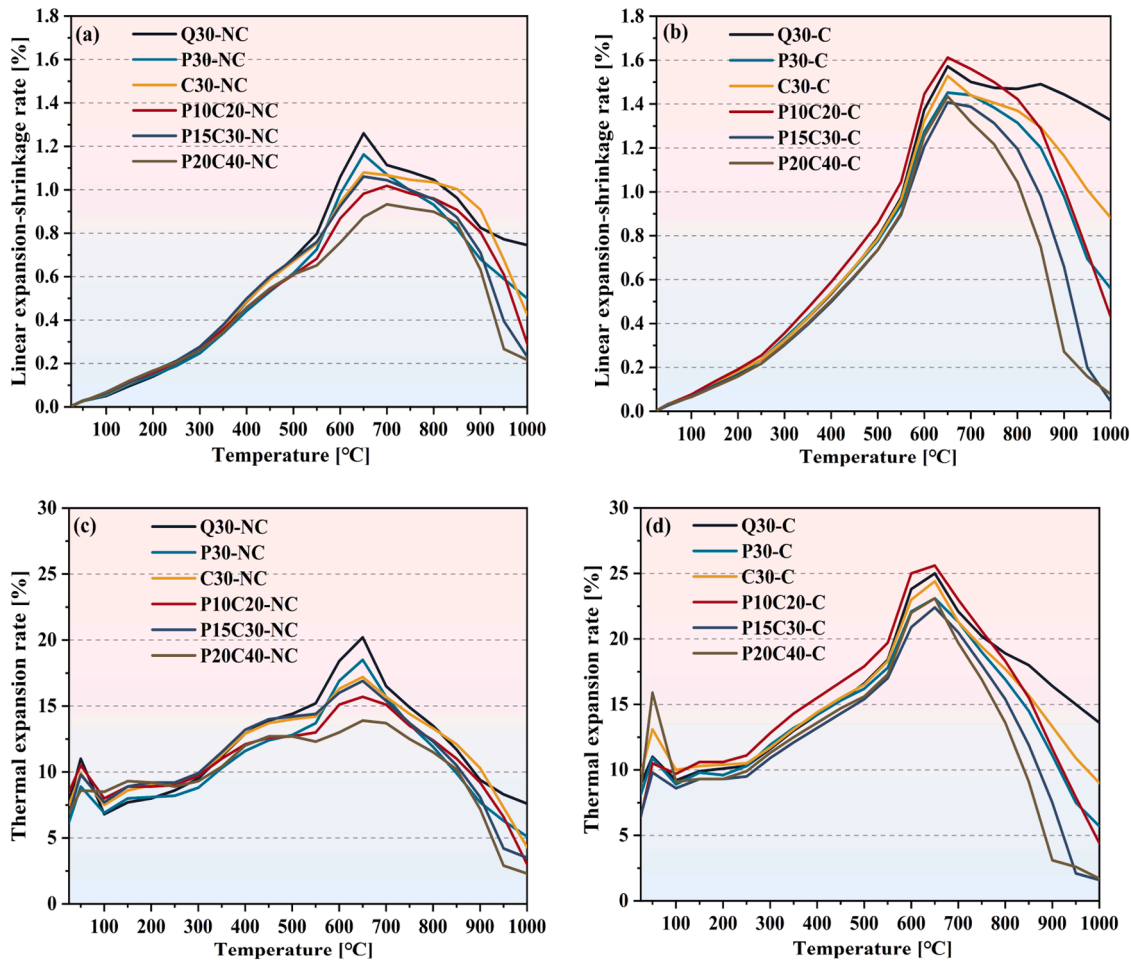


Fig. 14. (a)-(b) represent the linear expansion rate of specimens with different curing conditions at different temperatures; (c)-(d) represent the expansion rate of specimens with different curing conditions at different temperatures.

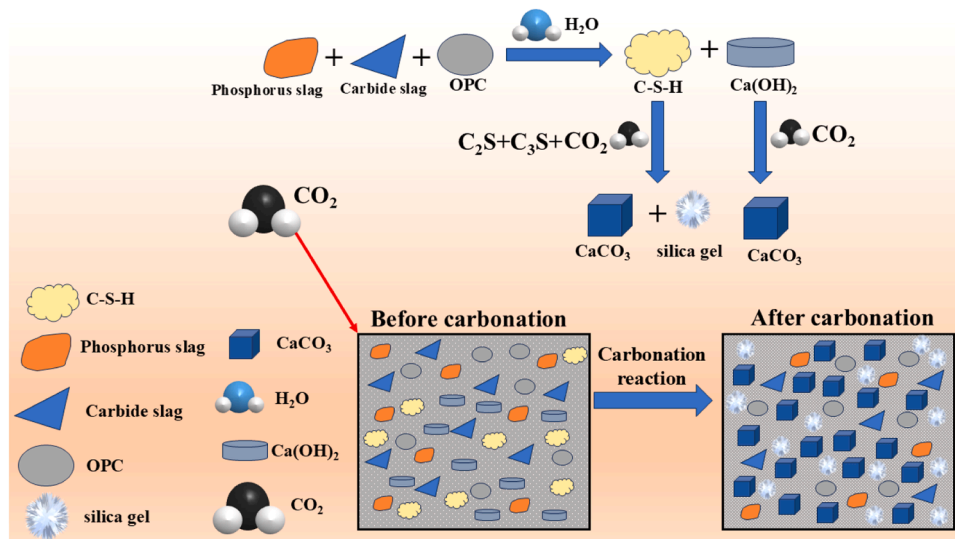


Fig. 15. Diagram of carbonation mechanism of PS, CS, and OPC.

fields. Technically, the high volcanic ash activity of PS and the rich calcium content of CS can jointly improve the mechanical properties and durability of cement-based materials and optimize the pore structure. Economically, since both are industrial by-products, they can

significantly reduce production costs and ease the pressure on resources and energy. Environmentally, large-scale utilization of these two wastes can reduce land use for storage, reduce the pollution of solid waste to the environment, and at the same time seal CO₂ in the environment,

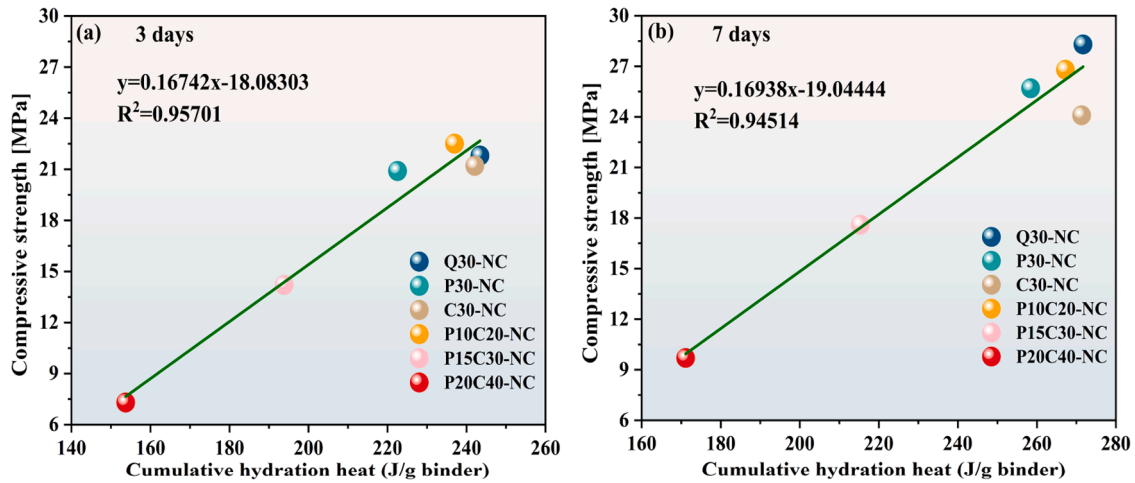


Fig. 16. Fitting relationship between cumulative hydration heat release and strength.

reducing carbon emissions from the cement industry to the environment. The coordinated use of the two can not only realize the efficient resource utilization of industrial waste slag, but also help promote the transformation of the cement industry towards a green and low-carbon direction.

4.1. Coupling mechanism of phosphorus slag-carbide slag-cement ternary binder in hydration

Fig. 16 is a fitting diagram of mechanical properties and hydration heat release. As shown in the figure, the strength has a high linear correlation with the cumulative hydration heat release [86]. Since CS can not only modify PS and mitigate the negative impacts of PS on hydration but also enhance the pozzolanic activity of PS to form additional calcium silicate hydrate gel, the degree of early hydration and strength performance of the P10C20-NC specimen are superior to those of the P30-NC specimen [35]. Due to the dilution effect of PS and CS, the cumulative hydration heat release and strength of P15C30-NC and P20C40-NC exhibit a decreasing trend.

During the hydration reaction stage, a comparison was made between the specimens containing PS and those in the control group with quartz addition. The results indicated that the incorporation of PS significantly extended the induction period of the paste, thereby delaying cement setting (refer to Fig. 3). This phenomenon primarily results from the residual phosphorus in the PS, which inhibits cement hydration. The mechanisms through which PS delays cement setting can be summarized as follows: (1) The retarding components, such as impurities like phosphorus and fluorine, form insoluble compounds that encase the cement surface, thereby impeding the hydration process. (2) Compounds produced from the interaction between these retarding components and Ca^{2+} ions in solution hinder the formation of CH crystals, leading to a reduced hydration rate. (3) A semi-permeable film that forms during the initial hydration of cement can adsorb onto the PS, resulting in a denser film that restricts the permeability of ions and water, further delaying the hydration process [30,49,87].

When the cement replacement ratio is the same (refer to Table 2), the induction period of the P10C20-NC specimen is significantly shorter. This effect may be attributed to two main factors: (1) CS enhances the pozzolanic activity of PS [35], resulting in more gel formation. (2) Following hydration, CS contributes a substantial amount of Ca^{2+} , which reacts with soluble phosphorus and fluorine in PS to produce insoluble phosphates and fluorides [31]. CS modifies PS through this reaction, thereby alleviating the negative impact of PS on matrix hydration and strength development. In the final phase of normal curing, the incorporation of CS decreased the amount of PS in the specimen,

resulting in the strength of the P10C20-NC specimen being lower than that of the P30-NC specimen.

4.2. Coupling mechanism of phosphorus slag - carbide slag - cement ternary binder in carbonation

During the carbonation curing process, PS reacts with CH to initiate a pozzolanic reaction. This reaction decreases the amounts of CH and pore-free water in the matrix, resulting in a faster carbonation rate for the P30-C specimen with PS compared to the Q30-C specimen containing quartz. At the same time, more CaCO_3 and low Ca/Si ratio gel will be formed in the later stage of carbonation [17]. Therefore, the specimen with only PS included is better than the one containing quartz in terms of carbonation rate and later carbonation strength (see Fig. 4 and Fig. 5). It is noteworthy that at the same cement replacement level, the P10C20-C specimen not only has higher strength than the P30-C specimen but also has a greater CO_2 absorption capacity (refer to Table 3). This can be attributed to the increased CH content in the P10C20-C matrix, which leads to an increase in CC generation following carbonation, thereby enhancing the strength and CO_2 absorption capacity of the specimen.

5. Conclusion

Through a series of tests, this experiment studied the influence mechanism of phosphorus slag on cement under different curing conditions and deeply explored the principle of how calcium carbide slag modifies phosphorus slag and the synergistic effect between the two. The research results show that:

- (1) The OPC-phosphorus slag-carbide slag ternary composite cement-based material has carbide slag that activates the pozzolanic activity of phosphorus slag, and the additional hydrated calcium silicate gel refines the microstructure of the matrix. At the same time, the additional active alumina in the phosphorus slag reacts with sulfate to generate more Aft. The synergistic effect of the two increases the strength of the matrix and improves the microstructure of the matrix. The pozzolanic reaction of the phosphorus slag consumes the free water and calcium hydroxide in the matrix, thereby increasing the carbonation rate of the matrix.
- (2) The large amount of Ca^{2+} produced in carbide slag can convert the soluble phosphorus and fluorine in the phosphorus slag into insoluble phosphates and fluorides, thereby weakening the negative impact of the phosphorus slag on the hydration of the matrix and achieving the purpose of modifying the phosphorus

slag; at the same time, it can improve the early strength and early hydration degree of the matrix of the ternary cement-based composite material.

- (3) OPC-phosphorus slag-carbide slag ternary cement-based composite material, due to the synergistic effect of phosphorus slag and carbide slag, promotes the consumption of calcium hydroxide in the matrix and also increases the carbonation rate of the matrix. In addition, the composite material has a higher carbon sequestration capacity, which plays a positive role in reducing carbon emissions in the cement industry.
- (4) The synergistic effect of phosphorus slag and carbide slag enables the OPC-phosphorus slag-carbide slag ternary cement composite material to produce additional calcium carbonate after carbonation, which not only improves the microstructure of the ternary cementitious material, but also enhances the mechanical properties of the material.

CRedit authorship contribution statement

Yue Wen-Ping: Writing – review & editing, Methodology, Investigation, Conceptualization. **Liao Yong-Pang:** Writing – review & editing, Resources, Project administration, Methodology, Investigation, Conceptualization. **Yang Yi:** Writing – review & editing, Resources, Project administration, Investigation, Conceptualization. **Liew Jia-Xiang:** Conceptualization, Investigation, Methodology, Project administration, Resources, Writing – review & editing. **Gao Rui-Cong:** Formal analysis, Investigation, Methodology, Project administration, Supervision, Writing – original draft. **Liu Fang:** Writing – review & editing, Investigation, Formal analysis. **Liu Guang-Min:** Writing – review & editing, Writing – original draft, Methodology, Investigation, Formal analysis.

Declaration of Competing Interest

The authors declare that they have no known competing financial interests or personal relationships that could have appeared to influence the work reported in this paper.

Acknowledgments

This research was supported by Kunming University of Science and Technology Graduate Top Innovative Talents Program (grant No. CA24163M037A), the Education Department of Shaanxi Provincial Government (Program No. 23JS059), and the Launch of Scientific Research in Xijing University (XJ21T01).

Data availability

Data will be made available on request.

References

- [1] T. Wu, S.T. Ng, J. Chen, Deciphering the CO₂ emissions and emission intensity of cement sector in China through decomposition analysis, *J. Clean. Prod.* 352 (2022) 131627, <https://doi.org/10.1016/j.jclepro.2022.131627>.
- [2] M.F. Kai, L.W. Zhang, K.M. Liew, New insights into creep characteristics of calcium silicate hydrates at molecular level, *Cem. Concr. Res.* 142 (2021) 106366, <https://doi.org/10.1016/j.cemconres.2021.106366>.
- [3] M. Sharma, S. Bishnoi, F. Martirena, K. Scrivener, Limestone calcined clay cement and concrete: a state-of-the-art review, *Cem. Concr. Res.* 149 (2021) 106564, <https://doi.org/10.1016/j.cemconres.2021.106564>.
- [4] Y. Li, H. Zhang, Z. Zhang, Y. Li, H. Fang, J. Yuan, S. Tang, The early-age cracking sensitivity, shrinkage, hydration process, pore structure and micromechanics of cement-based materials containing alkalis with different metal ions, *Dev. Built Environ.* 18 (2024) 100454, <https://doi.org/10.1016/j.dibe.2024.100454>.
- [5] Y. Yan, L. Tian, W. Zhao, S.A.M. Lazaro, X. Li, S. Tang, Dielectric and mechanical properties of cement pastes incorporated with magnetically aligned reduced graphene oxide, *Dev. Built Environ.* 18 (2024) 100471, <https://doi.org/10.1016/j.dibe.2024.100471>.
- [6] W. Zhang, M. Zhao, Z. Yang, R. Guo, X.-Y. Wang, R.-S. Lin, Properties of red sandstone-limestone-cement ternary composites: Hydration mechanism, microstructure, and high-temperature damage, *Dev. Built Environ.* 17 (2024) 100346, <https://doi.org/10.1016/j.dibe.2024.100346>.
- [7] O.E. Ige, D.V. Von Kallon, D. Desai, Carbon emissions mitigation methods for cement industry using a systems dynamics model, *Clean. Technol. Environ. Policy* 26 (3) (2024) 579–597, <https://doi.org/10.1007/s10098-023-02683-0>.
- [8] N. Yang, S. Xue, M.R. Ahmad, Q. Xuan, M.-F. Kai, J.-G. Dai, Development of red mud-modified geopolymer coating with radiative cooling effect for footway application, *J. Clean. Prod.* 450 (2024) 141915, <https://doi.org/10.1016/j.jclepro.2024.141915>.
- [9] W. Liu, L. Teng, S. Rohani, Z. Qin, B. Zhao, C.C. Xu, S. Ren, Q. Liu, B. Liang, CO₂ mineral carbonation using industrial solid wastes: a review of recent developments, *Chem. Eng. J.* 416 (2021) 129093, <https://doi.org/10.1016/j.cej.2021.129093>.
- [10] S. Liu, P. Rong, C. Zhang, J.-X. Lu, X. Guan, C. Shi, J. Zhu, Preparation and carbonation hardening of low calcium CO₂ sequestration materials from waste concrete powder and calcium carbide slag, *Cem. Concr. Compos.* 141 (2023) 105151, <https://doi.org/10.1016/j.cemconcomp.2023.105151>.
- [11] H. Mehdiadeh, X. Shao, K.H. Mo, T.-C. Ling, Enhancement of early age cementitious properties of yellow phosphorus slag via CO₂ aqueous carbonation, *Cem. Concr. Compos.* 133 (2022) 104702, <https://doi.org/10.1016/j.cemconcomp.2022.104702>.
- [12] B. Xu, Y. Yi, Treatment of ladle furnace slag by carbonation: Carbon dioxide sequestration, heavy metal immobilization, and strength enhancement, *Chemosphere* 287 (2022) 132274, <https://doi.org/10.1016/j.chemosphere.2021.132274>.
- [13] B. Xu, J. Qin, Y. Yi, Use of ladle slag for CO₂ sequestration and zinc immobilization, *Resour., Conserv. Recycl.* 199 (2023) 107220, <https://doi.org/10.1016/j.resconrec.2023.107220>.
- [14] Z. Geng, S. Tang, Y. Wang, H. A. Z. He, K. Wu, L. Wang, Stress relaxation properties of calcium silicate hydrate: a molecular dynamics study, *J. Zhejiang Univ. Sci. A* 25 (2) (2024) 97–115, <https://doi.org/10.1631/jzus.A2300476>.
- [15] L. Wang, M. Jin, S. Zhou, S. Tang, X. Lu, Investigation of microstructure of C-S-H and micro-mechanics of cement pastes under NH₄NO₃ dissolution by 29Si MAS NMR and microhardness, *Measurement* 185 (2021) 110019, <https://doi.org/10.1016/j.measurement.2021.110019>.
- [16] M.F. Kai, L.W. Zhang, K.M. Liew, Graphene and graphene oxide in calcium silicate hydrates: chemical reactions, mechanical behavior and interfacial sliding, *Carbon* 146 (2019) 181–193, <https://doi.org/10.1016/j.carbon.2019.01.097>.
- [17] B. Chen, M. Horgnies, B. Huet, V. Morin, K. Johannes, F. Kuznik, Comparative kinetics study on carbonation of ettringite and meta-ettringite based materials, *Cem. Concr. Res.* 137 (2020) 106209, <https://doi.org/10.1016/j.cemconres.2020.106209>.
- [18] Y. Shi, Q. Zhao, C. Xue, Y. Jia, W. Guo, Y. Zhang, Y. Qiu, Preparation and curing method of red mud-calcium carbide slag synergistically activated fly ash-ground granulated blast furnace slag based eco-friendly geopolymer, *Cem. Concr. Compos.* 139 (2023) 104999, <https://doi.org/10.1016/j.cemconcomp.2023.104999>.
- [19] Y. Liao, Z. Cai, F. Deng, J. Ye, K. Wang, S. Tang, Hydration behavior and thermodynamic modelling of ferroaluminate cement blended with steel slag, *J. Build. Eng.* 97 (2024) 110833, <https://doi.org/10.1016/j.jobe.2024.110833>.
- [20] Y. Liao, J. Yao, F. Deng, H. Li, K. Wang, S. Tang, Hydration behavior and strength development of supersulfated cement prepared by calcined phosphogypsum and slaked lime, *J. Build. Eng.* 80 (2023) 108075, <https://doi.org/10.1016/j.jobe.2023.108075>.
- [21] A. Allahverdi, M. Mahinroosta, Mechanical activation of chemically activated high phosphorous slag content cement, *Powder Technol.* 245 (2013) 182–188, <https://doi.org/10.1016/j.powtec.2013.04.037>.
- [22] X.W. Liu, L. Yang, B. Zhang, Utilization of phosphorus slag and fly ash for the preparation of ready-mixed mortar, *Appl. Mech. Mater.* 423–426 (2013) 987–992, <https://doi.org/10.4028/www.scientific.net/AMM.423-426.987>.
- [23] A. Allahverdi, S. Pilehvar, M. Mahinroosta, Influence of curing conditions on the mechanical and physical properties of chemically-activated phosphorous slag cement, *Powder Technol.* 288 (2016) 132–139, <https://doi.org/10.1016/j.powtec.2015.10.053>.
- [24] X. Xue, Y. Ke, Q. Kang, Q. Zhang, C. Xiao, F. He, Q. Yu, Cost-effective treatment of hemihydrate phosphogypsum and phosphorous slag as cemented paste backfill material for underground mine, *Adv. Mater. Sci. Eng.* 2019 (1) (2019), <https://doi.org/10.1155/2019/9087538>.
- [25] M.-F. Kai, G. Li, B.-B. Yin, A. Akbar, Aluminum-induced structure evolution and mechanical strengthening of calcium silicate hydrates: an atomistic insight, *Constr. Build. Mater.* 393 (2023) 132120, <https://doi.org/10.1016/j.conbuildmat.2023.132120>.
- [26] M.F. Kai, L.W. Zhang, K.M. Liew, Carbon nanotube-geopolymer nanocomposites: a molecular dynamics study of the influence of interfacial chemical bonding upon the structural and mechanical properties, *Carbon* 161 (2020) 772–783, <https://doi.org/10.1016/j.carbon.2020.02.014>.
- [27] P. Gao, X. Lu, C. Yang, X. Li, N. Shi, S. Jin, Microstructure and pore structure of concrete mixed with superfine phosphorous slag and superplasticizer, *Constr. Build. Mater.* 22 (5) (2008) 837–840, <https://doi.org/10.1016/j.conbuildmat.2006.12.015>.
- [28] Z. Zhang, Q. Wang, J. Yang, Hydration mechanisms of composite binders containing phosphorus slag at different temperatures, *Constr. Build. Mater.* 147 (2017) 720–732, <https://doi.org/10.1016/j.conbuildmat.2017.04.202>.
- [29] X. Chen, K. Fang, H. Yang, H. Peng, Hydration kinetics of phosphorous slag-cement paste, *J. Wuhan. Univ. Technol. Mater. Sci. Ed.* 26 (1) (2011) 142–146, <https://doi.org/10.1007/s11595-011-0186-4>.

- [30] X. Chen, L. Zeng, K. Fang, Anti-crack performance of phosphorus slag concrete, *Wuhan. Univ. J. Nat. Sci.* 14 (1) (2009) 80–86, <https://doi.org/10.1007/s11859-009-0117-9>.
- [31] S. Liu, P. Fang, J. Ren, S. Li, Application of lime neutralised phosphogypsum in supersulfated cement, *J. Clean. Prod.* 272 (2020) 122660, <https://doi.org/10.1016/j.jclepro.2020.122660>.
- [32] H. Mehdizadeh, E. Najafi Kani, A. Palomo Sanchez, A. Fernandez-Jimenez, Rheology of activated phosphorus slag with lime and alkaline salts, *Cem. Concr. Res.* 113 (2018) 121–129, <https://doi.org/10.1016/j.cemconres.2018.07.010>.
- [33] W. Li, Y. Yi, Use of carbide slag from acetylene industry for activation of ground granulated blast-furnace slag, *Constr. Build. Mater.* 238 (2020) 117713, <https://doi.org/10.1016/j.conbuildmat.2019.117713>.
- [34] C.L. Yong, K.H. Mo, S. Koting, Phosphorus slag in supplementary cementitious and alkali activated materials: a review on activation methods, *Constr. Build. Mater.* 352 (2022) 129028, <https://doi.org/10.1016/j.conbuildmat.2022.129028>.
- [35] S. Cui, K. Fan, Y. Yao, Preparation and characterization of quaternary clinker-free cementitious materials containing phosphorus slag, calcium carbide slag, desulfurization gypsum, and metakaolin, *Constr. Build. Mater.* 411 (2024) 134602, <https://doi.org/10.1016/j.conbuildmat.2023.134602>.
- [36] J. Bawab, H. El-Hassan, A. El-Dieb, J. Khatib, Accelerated carbonation curing of concrete incorporating calcium carbide residue, *J. Build. Eng.* 88 (2024) 109258, <https://doi.org/10.1016/j.jobe.2024.109258>.
- [37] Y. Su, H. Zhao, X. He, Z. Zheng, Q. Ma, J. Ding, M. Bao, The effect of wet-grinding phosphorus slag on the hydration kinetics of Portland cement, *Constr. Build. Mater.* 364 (2023) 129942, <https://doi.org/10.1016/j.conbuildmat.2022.129942>.
- [38] A. Sai, W. Baomin, C. Wenxiu, The cementitious properties of alkali-activated municipal solid waste incineration fly ash-phosphorus slag-secondary aluminum dross matrix composites and the mechanism of solidification of heavy metals, *Constr. Build. Mater.* 438 (2024) 137254, <https://doi.org/10.1016/j.conbuildmat.2024.137254>.
- [39] Y. Yahui, X. Gang, T. Bin, Carbonation characteristics of cement-based materials under the uniform distribution of pore water, *Constr. Build. Mater.* 275 (2021) 121450, <https://doi.org/10.1016/j.conbuildmat.2020.121450>.
- [40] C.J. Abo, A. Astm, 349-97. Standard test method for compressive strength of hydraulic-cement mortars (using portions of prisms broken in flexure), 4 (2002).
- [41] G. Huang, R. Gao, X.-Y. Wang, R. Guo, Y. Han, R.-S. Lin, Production of low-carbon cement composites using red sandstone: CO2 storage and performance analysis, *Constr. Build. Mater.* 449 (2024) 138323, <https://doi.org/10.1016/j.conbuildmat.2024.138323>.
- [42] R. Snellings, J. Chwast, Ö. Cizer, N. De Belie, Y. Dhandapani, P. Durdzinski, J. Elsen, J. Haufe, D. Hooton, C. Patapy, M. Santhanam, K. Scrivener, D. Snoeck, L. Steger, S. Tongbo, A. Vollpracht, F. Winnefeld, B. Lothenbach, RILEM TC-238 SCM recommendation on hydration stoppage by solvent exchange for the study of hydrate assemblages, *Mater. Struct.* 51 (6) (2018), <https://doi.org/10.1617/s11527-018-1298-5>.
- [43] R.-S. Lin, X.-Y. Wang, H. Yi, Effects of cement types and addition of quartz and limestone on the normal and carbonation curing of cement paste, *Constr. Build. Mater.* 305 (2021), <https://doi.org/10.1016/j.conbuildmat.2021.124799>.
- [44] Q.T. Phung, N. Maes, D. Jacques, E. Bruneel, I. Van Driessche, G. Ye, G. De Schutter, Effect of limestone fillers on microstructure and permeability due to carbonation of cement pastes under controlled CO2 pressure conditions, *Constr. Build. Mater.* 82 (2015) 376–390, <https://doi.org/10.1016/j.conbuildmat.2015.02.093>.
- [45] R.-S. Lin, X.-Y. Wang, H. Yi, Effects of cement types and addition of quartz and limestone on the normal and carbonation curing of cement paste, *Constr. Build. Mater.* 305 (2021) 124799, <https://doi.org/10.1016/j.conbuildmat.2021.124799>.
- [46] M.-Y. Xuan, R. Guo, R.-S. Lin, X. Wang, X.-Y. Wang, Mechanism of fineness and content of quartz powder on the improvement of carbonation curing efficiency, *Cem. Concr. Compos.* 150 (2024), <https://doi.org/10.1016/j.cemconcomp.2024.105570>.
- [47] G. Huang, Y. Lv, S. Ren, Y. Liao, X.-Y. Wang, R. Guo, R.-S. Lin, Production of low-CO2 ternary binder using red sandstone, cement, and granulated blast furnace slag: a comprehensive performance analysis, *Constr. Build. Mater.* 431 (2024), <https://doi.org/10.1016/j.conbuildmat.2024.136576>.
- [48] Y. Shan, L. Zhang, L. Liu, Study on the macroscopic properties of phosphorus slag composite cementitious materials based on hydration perspective, *J. Build. Eng.* 78 (2023) 107741, <https://doi.org/10.1016/j.jobe.2023.107741>.
- [49] L. Dong-xu, C. Lin, X. Zhong-zi, L. Zhi-min, A blended cement containing blast furnace slag and phosphorus slag, *J. Wuhan. Univ. Technol. Mater. Sci. Ed.* 17 (2) (2002) 62–65, <https://doi.org/10.1007/BF02832625>.
- [50] Y. He, Y. Liu, X. Liu, M. Lan, B. Lei, Q. Chen, X. Xue, Mechanical properties of eco-cement mortar containing MgO-modified phosphorus slag, *Constr. Build. Mater.* 428 (2024), <https://doi.org/10.1016/j.conbuildmat.2024.136223>.
- [51] Y. Peng, J. Zhang, J. Liu, J. Ke, F. Wang, Properties and microstructure of reactive powder concrete having a high content of phosphorus slag powder and silica fume, *Constr. Build. Mater.* 101 (2015) 482–487, <https://doi.org/10.1016/j.conbuildmat.2015.10.046>.
- [52] M. Thierry, G. Villain, P. Dangla, G. Platret, Investigation of the carbonation front shape on cementitious materials: effects of the chemical kinetics, *Cem. Concr. Res.* 37 (7) (2007) 1047–1058, <https://doi.org/10.1016/j.cemconres.2007.04.002>.
- [53] Z. Liu, W. Meng, Fundamental understanding of carbonation curing and durability of carbonation-cured cement-based composites: a review, *J. CO2 Util.* 44 (2021) 101428, <https://doi.org/10.1016/j.jcou.2020.101428>.
- [54] D. Zhang, Z. Ghoulleh, Y. Shao, Review on carbonation curing of cement-based materials, *J. CO2 Util.* 21 (2017) 119–131, <https://doi.org/10.1016/j.jcou.2017.07.003>.
- [55] Y. Liao, M. Shi, R. Gao, F. Ma, R.-S. Lin, Y. Lv, Z. Chen, Preliminary exploration of the hydration-carbonation coupling mechanism of low-carbon calcined clay-carbide slag-cement composites, *J. CO2 Util.* 85 (2024) 102876, <https://doi.org/10.1016/j.jcou.2024.102876>.
- [56] W. Ashraf, Carbonation of cement-based materials: challenges and opportunities, *Constr. Build. Mater.* 120 (2016) 558–570, <https://doi.org/10.1016/j.conbuildmat.2016.05.080>.
- [57] H. Bensalah, M.F. Bekheet, S. Alami Younsi, M. Ouammou, A. Gurlo, Hydrothermal synthesis of nanocrystalline hydroxyapatite from phosphogypsum waste, *J. Environ. Chem. Eng.* 6 (1) (2018) 1347–1352, <https://doi.org/10.1016/j.jece.2018.01.052>.
- [58] G. Liu, Y. Liao, X. Sha, G. Liu, Y. Zhang, R. Guo, Y. Yue, Application of calcium sulfate whiskers to cement-based materials: a review, *Materials* (2024).
- [59] A. Ipavec, R. Gabrovšek, T. Vuk, V. Kaučič, J. Maček, A. Meden, Carboaluminate phases formation during the hydration of calcite-containing portland cement, *J. Am. Ceram. Soc.* 94 (4) (2011) 1238–1242, <https://doi.org/10.1111/j.1551-2916.2010.04201.x>.
- [60] L.G. Baquerizo, T. Matschei, K.L. Scrivener, M. Saeidpour, L. Wadsö, Hydration states of AFm cement phases, *Cem. Concr. Res.* 73 (2015) 143–157, <https://doi.org/10.1016/j.cemconres.2015.02.011>.
- [61] X. Hu, P. He, C. Shi, Carbonate binders: historic developments and perspectives, *Cem. Concr. Res.* 175 (2024) 107352, <https://doi.org/10.1016/j.cemconres.2023.107352>.
- [62] T. Petit, L. Puskar, FTIR spectroscopy of nanodiamonds: methods and interpretation, *Diam. Relat. Mater.* 89 (2018) 52–66, <https://doi.org/10.1016/j.diamond.2018.08.005>.
- [63] Y. Liao, Y. Lv, G. Huang, S. Ren, X.-Y. Wang, R. Guo, Y. Tian, S. Deng, R.-S. Lin, Strength and microstructure analysis of subgrade materials containing red sandstone-limestone-cement composites and red sandstone gravel, *Constr. Build. Mater.* 416 (2024), <https://doi.org/10.1016/j.conbuildmat.2024.135190>.
- [64] A. Akbar, K.M. Liew, Influence of elevated temperature on the microstructure and mechanical performance of cement composites reinforced with recycled carbon fibers, *Compos. Part B: Eng.* 198 (2020) 108245, <https://doi.org/10.1016/j.compositesb.2020.108245>.
- [65] L. Hu, Y. Jia, Z. Chen, Y. Yao, J. Sun, Q. Xie, H. Yang, An insight of carbonation-hydration kinetics and microstructure characterization of cement paste under accelerated carbonation at early age, *Cem. Concr. Compos.* 134 (2022) 104763, <https://doi.org/10.1016/j.cemconcomp.2022.104763>.
- [66] J. Chen, Y. Li, H. Zhou, Y. Li, H. Guo, Nuclear magnetic resonance study on concrete pore structure evolution under different curing environments, *JOM* 74 (5) (2022) 1819–1827, <https://doi.org/10.1007/s11837-022-05221-3>.
- [67] L. Li, X.-B. Zuo, C. Wang, D. Cui, Modelling of water sorption hysteresis of cement-based materials based on pore microstructure, *J. Build. Eng.* 98 (2024) 111025, <https://doi.org/10.1016/j.jobe.2024.111025>.
- [68] S. Liu, L. Wang, Investigation on strength and pore structure of supersulfated cement paste, *Mater. Sci.* 24 (2018), <https://doi.org/10.5755/j01.ms.24.3.18300>.
- [69] J. Yang, H. Hu, X. He, Y. Su, Y. Wang, H. Tan, H. Pan, Effect of steam curing on compressive strength and microstructure of high volume ultrafine fly ash cement mortar, *Constr. Build. Mater.* 266 (2021) 120894, <https://doi.org/10.1016/j.conbuildmat.2020.120894>.
- [70] B. Song, S. Liu, X. Hu, K. Ouyang, G. Li, C. Shi, Compressive strength, water and chloride transport properties of early CO2-cured Portland cement-fly ash-slag ternary mortars, *Cem. Concr. Compos.* 134 (2022) 104786, <https://doi.org/10.1016/j.cemconcomp.2022.104786>.
- [71] S. Liu, L. Wang, B. Yu, Effect of modified phosphogypsum on the hydration properties of the phosphogypsum-based supersulfated cement, *Constr. Build. Mater.* 214 (2019) 9–16, <https://doi.org/10.1016/j.conbuildmat.2019.04.052>.
- [72] B. Guo, G. Chu, R. Yu, Y. Wang, Q. Yu, D. Niu, Effects of sufficient carbonation on the strength and microstructure of CO2-cured concrete, *J. Build. Eng.* 76 (2023) 107311, <https://doi.org/10.1016/j.jobe.2023.107311>.
- [73] X. Lv, Y. Shi, Y. Wang, J. Li, Utilization of phosphorus slag as fly ash replacement in low-heat Portland cement blends: comparative study of hydration behaviors, physical properties, and life-cycle assessment, *Constr. Build. Mater.* 396 (2023) 132346, <https://doi.org/10.1016/j.conbuildmat.2023.132346>.
- [74] X. Shen, P. Feng, Q. Zhang, Y. Cai, C. Chen, X. Han, W. Zhu, J. Hong, J. Chen, The key role of water on the transformation of the precursors to nano-crystalline C-S-H, *Compos. Part B: Eng.* 283 (2024) 111601, <https://doi.org/10.1016/j.compositesb.2024.111601>.
- [75] X. Ouyang, X. Li, J. Li, Y. Ma, M. Zhang, Z. Li, J. Fu, Multiscale microstructure and reactivity evolution of recycled concrete fines under gas-solid carbonation, *Cem. Concr. Compos.* (2024) 105903, <https://doi.org/10.1016/j.cemconcomp.2024.105903>.
- [76] S. Ren, G. Huang, W. Zhang, X. Sha, G. Liu, R.-S. Lin, L. Chen, Enhancing cement-based materials hydration and carbonation efficiency with pre-carbonated lime mud, *J. CO2 Util.* 88 (2024) 102928, <https://doi.org/10.1016/j.jcou.2024.102928>.
- [77] R.-S. Lin, G. Huang, F.-Y. Ma, T.-H. Pan, X.-Y. Wang, Y. Han, Y.-P. Liao, Investigation of phosphogypsum-based cementitious materials: the effect of lime modification, *Dev. Built Environ.* 18 (2024) 100477, <https://doi.org/10.1016/j.dibe.2024.100477>.
- [78] R.-S. Lin, Y. Han, X.-Y. Wang, Macro-meso-micro experimental studies of calcined clay limestone cement (LC3) paste subjected to elevated temperature, *Cem. Concr. Compos.* 116 (2021) 103871, <https://doi.org/10.1016/j.cemconcomp.2020.103871>.

- [79] M.C.R. Farage, J. Sercombe, C. Gallé, Rehydration and microstructure of cement paste after heating at temperatures up to 300 °C, *Cem. Concr. Res.* 33 (7) (2003) 1047–1056, [https://doi.org/10.1016/S0008-8846\(03\)00005-X](https://doi.org/10.1016/S0008-8846(03)00005-X).
- [80] S. Lim, P. Mondal, Micro- and nano-scale characterization to study the thermal degradation of cement-based materials, *Mater. Charact.* 92 (2014) 15–25, <https://doi.org/10.1016/j.matchar.2014.02.010>.
- [81] S. Ghabezloo, Effect of porosity on the thermal expansion coefficient: a discussion of the paper ‘Effects of mineral admixtures on the thermal expansion properties of hardened cement paste’ by Z.H. Shui, R. Zhang, W. Chen, D. Xuan, *Constr. Build. Mater.* 24 (9) (2010) 1761–1767, *Constr. Build. Mater.* 24 (9) (2010) 1796–1798, <https://doi.org/10.1016/j.conbuildmat.2010.03.006>.
- [82] M. Malik, S.K. Bhattacharyya, S.V. Barai, Thermal and mechanical properties of concrete and its constituents at elevated temperatures: a review, *Constr. Build. Mater.* 270 (2021) 121398, <https://doi.org/10.1016/j.conbuildmat.2020.121398>.
- [83] X. Cong, R.J. Kirkpatrick, Effects of the temperature and relative humidity on the structure of CSH gel, *Cem. Concr. Res.* 25 (6) (1995) 1237–1245, [https://doi.org/10.1016/0008-8846\(95\)00116-T](https://doi.org/10.1016/0008-8846(95)00116-T).
- [84] Q. Zhou, F.P. Glasser, Thermal stability and decomposition mechanisms of ettringite at < 120°C, *Cem. Concr. Res.* 31 (9) (2001) 1333–1339, [https://doi.org/10.1016/S0008-8846\(01\)00558-0](https://doi.org/10.1016/S0008-8846(01)00558-0).
- [85] J. Chen, J. Jia, M. Zhu, Understanding the effect of alkali content on hydration, hardening, and performance of Portland cement – a comprehensive review, *Mater. Today Commun.* 40 (2024) 109728, <https://doi.org/10.1016/j.mtcomm.2024.109728>.
- [86] Z. Li, D. Lu, X. Gao, Analysis of correlation between hydration heat release and compressive strength for blended cement pastes, *Constr. Build. Mater.* 260 (2020) 120436, <https://doi.org/10.1016/j.conbuildmat.2020.120436>.
- [87] L. Dongxu, S. Jinlin, C. Lin, W. Xuequan, The influence of fast-setting/early-strength agent on high phosphorous slag content cement, *Cem. Concr. Res.* 31 (1) (2001) 19–24, [https://doi.org/10.1016/S0008-8846\(00\)00442-7](https://doi.org/10.1016/S0008-8846(00)00442-7).